IMMUNOLOGY

Systems approach reveals distinct and shared signaling networks of the four PGE_2 receptors in T cells

Anna M. Lone[1,2,3†], Piero Giansanti[4,5], Marthe Jøntvedt Jørgensen[2,3], Enio Gjerga[6,7], Aurelien Dugourd[6,7], Arjen Scholten[4‡], Julio Saez-Rodriguez[6,7], Albert J. R. Heck[4], Kjetil Taskén[1,2,3]*

Prostaglandin E_2 (PGE_2) promotes an immunosuppressive microenvironment in cancer, partly by signaling through four receptors (EP_1, EP_2, EP_3, and EP_4) on T cells. Here, we comprehensively characterized PGE_2 signaling networks in helper, cytotoxic, and regulatory T cells using a phosphoproteomics and phosphoflow cytometry approach. We identified ~1500 PGE_2-regulated phosphosites and several important $EP_{1–4}$ signaling nodes, including PKC, CK2, PKA, PI3K, and Src. T cell subtypes exhibited distinct signaling pathways, with the strongest signaling in EP_2-stimulated $CD8^+$ cells. EP_2 and EP_4, both of which signal through $G_{\alpha s}$, induced similar signaling outputs, but with distinct kinetics and intensity. Functional predictions from the observed phosphosite changes revealed PGE_2 regulation of key cellular and immunological processes. Last, network modeling suggested signal integration between the receptors and a substantial contribution from G protein–independent signaling. This study offers a comprehensive view of the different PGE_2-regulated phosphoproteomes in T cell subsets, providing a valuable resource for further research on this physiologically and pathophysiologically important signaling system.

INTRODUCTION

Prostaglandin E_2 (PGE_2) is the most abundant prostanoid in the human body and plays a crucial role in maintaining immune homeostasis as well as in pathophysiological settings, including cancer and chronic inflammatory conditions (*1*, *2*). PGE_2 is increased in colorectal, lung, breast, and pancreatic cancers (*3*), where it is produced by tumor cells or induced regulatory T cells (T_{regs}) (*4*) and promotes tumor growth by stimulating angiogenesis, cell invasion, and metastasis while inhibiting tumor cell apoptosis (*5*). PGE_2 also contributes to the formation of an immunosuppressive tumor microenvironment through effects on multiple immune cell types (*6–13*).

Because of its significance in cancer, methods for interfering with PGE_2 signaling are being explored as cancer prevention and treatment. In particular, inhibition of cyclooxygenase 1 (COX1) and COX2, which control the rate-limiting step in the biosynthesis of PGE_2, reduces the incidence of colorectal cancer (*14–16*) and improves survival if treatment is initiated after diagnosis (*17*, *18*). Individual PGE_2 receptors—in particular, EP_1, EP_2, and EP_4—have also been targeted with antagonists for increased specificity (*19*, *20*). There also appears to be synergy between PGE_2 targeting and cancer immunotherapy. For instance, COX inhibitors enhance the effect of immune checkpoint blockade (*21*), and a peptide that blocks an inhibitory PGE_2 signaling pathway augments the antitumor efficacy of chimeric antigen receptor T cells (*22*). There is also interest in combining EP antagonists with immunotherapy, and a selective EP_4 antagonist is now in phase 1 clinical trials (ClinicalTrials.gov, NCT03155061) (*23*) in combination with nivolumab in patients with solid tumors. There is thus ample basis for pursuing PGE_2-targeted cancer therapy alone or in combination with other immunotherapies. However, given the plethora of tissue-, cell-, and receptor-specific effects of PGE_2 in health and disease, it is crucial to have a comprehensive understanding of the signaling events and biological functions regulated by PGE_2 to avoid unintended side effects of blocking specific PGE_2-regulated pathways.

PGE_2 signals through four distinct G protein–coupled receptors (GPCRs): EP_1, EP_2, EP_3, and EP_4 (*19*, *24*), all of which appear to be present on T cells, with EP_2 and EP_4 being the most highly abundant (*25–27*). EP_1 is $G_{\alpha q}$-linked and signals mainly through phospholipase C (PLC), leading, in turn, to protein kinase C (PKC) activation (*2*, *20*, *24*). EP_2 and EP_4 both couple to the stimulatory G protein, $G_{\alpha s}$, which activates adenylyl cyclase, thereby increasing intracellular cyclic adenosine monophosphate (cAMP), which, in turn, activates protein kinase A (PKA). In addition, EP_4 couples to $G_{\alpha i}$, which inhibits PKA and is also associated with the release of the βγ subunits of the G protein complex, thus triggering phosphoinositide 3-kinase (PI3K) signaling (*28–30*). EP_3 couples mainly with $G_{\alpha i}$, but it exists in multiple isoforms, some of which couple to alternative G_α proteins and pathways (*20*, *24*). These receptors also signal through G protein–independent pathways such as β-arrestin signaling (*31–36*). Together, these myriad intracellular signaling options resulting from one extracellular stimulus present an interesting problem in signal integration and functional output.

We have been particularly interested in PGE_2 signaling in T cells because this plays an important role in many pathophysiological settings, including cancer and chronic inflammatory conditions (*1*, *2*, *37*). PGE_2 suppresses immune function by promoting T_{reg} generation, recruitment, and proliferation (*9*, *38*); by inhibiting $CD8^+$ T cell cytotoxicity by stimulating the production of CD94-NKG2A heterodimers (CD94/NKG2A) (*39*); by inhibiting T cell receptor (TCR)–dependent interferon γ release from $CD8^+$ T cells (*40*); and by promoting a shift from an antitumor T helper type 1 (T_H1) response

[1]Department of Cancer Immunology, Institute of Cancer Research, Oslo University Hospital, 0424 Oslo, Norway. [2]K.G. Jebsen Centre for Cancer Immunotherapy and K.G. Jebsen Centre for B Cell Malignancies, Institute of Clinical Medicine, University of Oslo, 0317 Oslo, Norway. [3]Centre for Molecular Medicine Norway, Nordic EMBL Partnership, University of Oslo, 0318 Oslo, Norway. [4]Biomolecular Mass Spectrometry and Proteomics, Utrecht Institute for Pharmaceutical Sciences and Bijvoet Center for Biomolecular Research, University of Utrecht, 3584 CH Utrecht, Netherlands. [5]Chair of Proteomics and Bioanalytics, Technical University of Munich, Freising 85354, Germany. [6]Joint Research Centre for Computational Biomedicine (JRC-Combine), RWTH-Aachen University Hospital, Faculty of Medicine, Aachen 52074, Germany. [7]Faculty of Medicine, Institute for Computational Biomedicine, Heidelberg University Hospital, Bioquant, Heidelberg University, Heidelberg 69120, Germany.
*Corresponding author. Email: kjetil.tasken@medisin.uio.no
†Present address: Norwegian Medicines Agency, 0663 Oslo, Norway.
‡Present address: UniQure, 1105 BP Amsterdam, Netherlands.

to an immunosuppressive T_H2 response (*9*, *41*). In addition, our laboratory has characterized a PGE_2-regulated inhibitory cAMP-PKA pathway in effector T (T_{eff}) cells with importance in disease (*1*, *4*, *42*–*47*). PGE_2 can also have a proinflammatory, cancer-promoting function in T cells (*2*, *48*). For instance, PGE_2 promotes interleukin 23 (IL-23)–induced T_H17 differentiation and proliferation (*26*, *49*–*51*), induces T_H1 differentiation through a PI3K-Akt signaling pathway when strong TCR signaling is also present (*50*), and promotes T cell proliferation through the induction of costimulatory molecules on dendritic cells (*52*).

We have previously studied PGE_2 signaling pathways in primary ($CD3^+$) T cells using phosphoproteomics (*53*), and a few other mass spectrometry (MS)–based studies on PGE_2 stimulation have been performed in Jurkat T cells (*54*, *55*) and fibroblasts (*56*). In these studies, all four EPs were stimulated concurrently by PGE_2, so that the individual contributions of each receptor could not be assessed. In a normal physiological context, PGE_2 would, of course, be the natural stimulus for this receptor system, and signaling would proceed through each of the receptors that is present on an individual cell. However, given the interest in targeting specific receptors in cancer therapy and other conditions, as well as an academic interest from a signaling network perspective in understanding how this four-receptor system integrates signals from individual receptors, it would also be valuable to have a better understanding of the specific signaling occurring through each receptor. Here, we therefore chart, in a system-wide manner, the signaling elicited by each of the four PGE_2 receptors individually to obtain a detailed map of the EP signalosomes and comprehensive PGE_2-regulated phosphoproteomes in primary T cell subtypes, including helper ($CD4^+$) T cells, cytotoxic ($CD8^+$) T cells, and T_{regs}. To this end, we stimulated cells with receptor-specific agonists and studied the signaling that was elicited using MS-based phosphoproteomics and multiplexed phosphoflow cytometry. Here, we present a global and detailed view of the signaling nodes, pathways, and networks regulated in $CD4^+$ T cells, $CD8^+$ T cells, and T_{regs} upon triggering EP_1, EP_2, EP_3, or EP_4. This system-wide view of the contributions from and cross-talk between the different receptors sheds light on an important immunoregulatory network and provides a context in which the systems pharmacology of targeting PGE_2 or its receptors can be assessed. Further, the current study provides a valuable resource for targeted studies of PGE_2 signaling mechanisms and biological functions in T cells.

RESULTS

PGE_2 receptors $EP_{1–4}$ regulate unique and overlapping phosphosites in T cell subsets

To map the PGE_2-regulated phosphoproteome in T cells, we stimulated $CD4^+$ T cells, $CD8^+$ T cells, and T_{regs} from healthy donors with agonists highly specific for each receptor (table S1) or PGE_2 and then performed phosphoproteomics using a label-free strategy with Ti^{4+}-immobilized metal ion affinity chromatography (IMAC) enrichment (fig. S1, A to E) (*55*). In total, we identified more than 21,000 phosphopeptides (data file S1) and quantified 5000 to 8000 unique phosphosites with very high reproducibility across each studied cell type. The Pearson correlation coefficients between biological replicates were between 0.7 and 0.96, and for a given condition, about 50 to 60% of the phosphosites could be quantified in each of the five biological replicates (fig. S2). The quantitative analysis revealed a stronger and distinct response in $CD8^+$ cells compared to $CD4^+$ cells and T_{regs} (Fig. 1, A to C). In particular, we observed regulation (an increase or decrease in phosphorylation) of more than 1000 phosphosites upon stimulation of $CD8^+$ T cells with the EP_2 agonist (Fig. 1D). In this cell type, more regulated sites were observed when stimulating with EP_2 agonist than with PGE_2, likely due to the inhibitory effect on $G_{\alpha s}$ signaling of simultaneous PGE_2 signaling through the $G_{\alpha i}$-coupled EP_3 receptor. In terms of signaling differences between cell types, the lower number of regulated sites in T_{regs} may be due to the high basal amounts of cAMP in this cell type (*57*), which could dampen the cAMP-dependent arm of the PGE_2 response. The phosphoproteomes regulated by the different receptors in a given cell type showed substantial overlap, indicating cross-talk and possible signal integration between receptors. However, many regulated phosphosites were unique to each receptor (Fig. 1E and fig. S3, A and B). For instance, in $CD8^+$ cells, the EP_2 receptor uniquely regulated 706 phosphosites, and in addition, regulated 398 sites that were also regulated by one or more of the other receptors. Thus, both unique and shared signaling pathways are present downstream of the individual receptors.

Identifying kinases that control the PGE_2-regulated phosphoproteomes

To further understand how the EP-regulated phosphoproteomes are controlled, we used NetPhorest (*58*) to predict which kinases phosphorylate the regulated phosphosites (Fig. 1F, fig S4, and table S2). In both $CD8^+$ and $CD4^+$ cells, the PKC, cyclin-dependent kinase (CDK), CDK-like kinase (CLK), casein kinase 2 (CK2), and mitogen-activated protein kinase (MAPK) groups were the most highly predicted. PKA, which is known to be a key regulator of PGE_2 signaling, was also highly predicted in each cell type. Although the absolute number of predictions for a given kinase varied between cell types, the patterns in the predicted kinases between different stimulation conditions (receptor-specific agonist or PGE_2) remained similar. The sequence motifs of the regulated phosphosites were then examined using IceLogos and corresponded well with the predicted kinases. The predominant IceLogo for the regulated phosphosites was RRXSP for all stimulation conditions (Fig. 1G, top row, and fig. S5), with some variations between stimulation conditions and cell types. Surmising that this logo is likely a composite of multiple motifs, we isolated all regulated sites with proline in the +1 position (Fig. 1G, bottom row left, and fig. S6) and found that these sites often also contained a proline in the −2 position. This would agree well with phosphorylation sites for extracellular signal–regulated kinase 1 (ERK1; also known as MAPK3), ERK2 (also known as MAPK1), or CDK2, CDK4, or CDK5 (*59*), all of which are kinases predicted by NetPhorest.

For the regulated phosphosites without proline in position +1 (Fig. 1G, bottom row right, and fig. S7), a strong RRXpS motif emerged in $CD8^+$ cells, likely accounting for the PKA prediction. In contrast, in nonproline phosphosites that increased in abundance upon stimulation in $CD4^+$ cells, we mainly observed a different motif, pSDXE (fig. S7), which is consistent with CK2 phosphorylation (*60*). This corroborates the prediction from NetPhorest that there is a higher relative proportion of CK2 phosphorylation events in $CD4^+$ cells than in $CD8^+$ cells. In general, phosphorylation motifs and kinase predictions were similar between stimulation conditions and cell types, implying that the signaling pathways originating from each receptor proceed through many of the same kinase nodes, allowing for receptor cross-talk and signal integration.

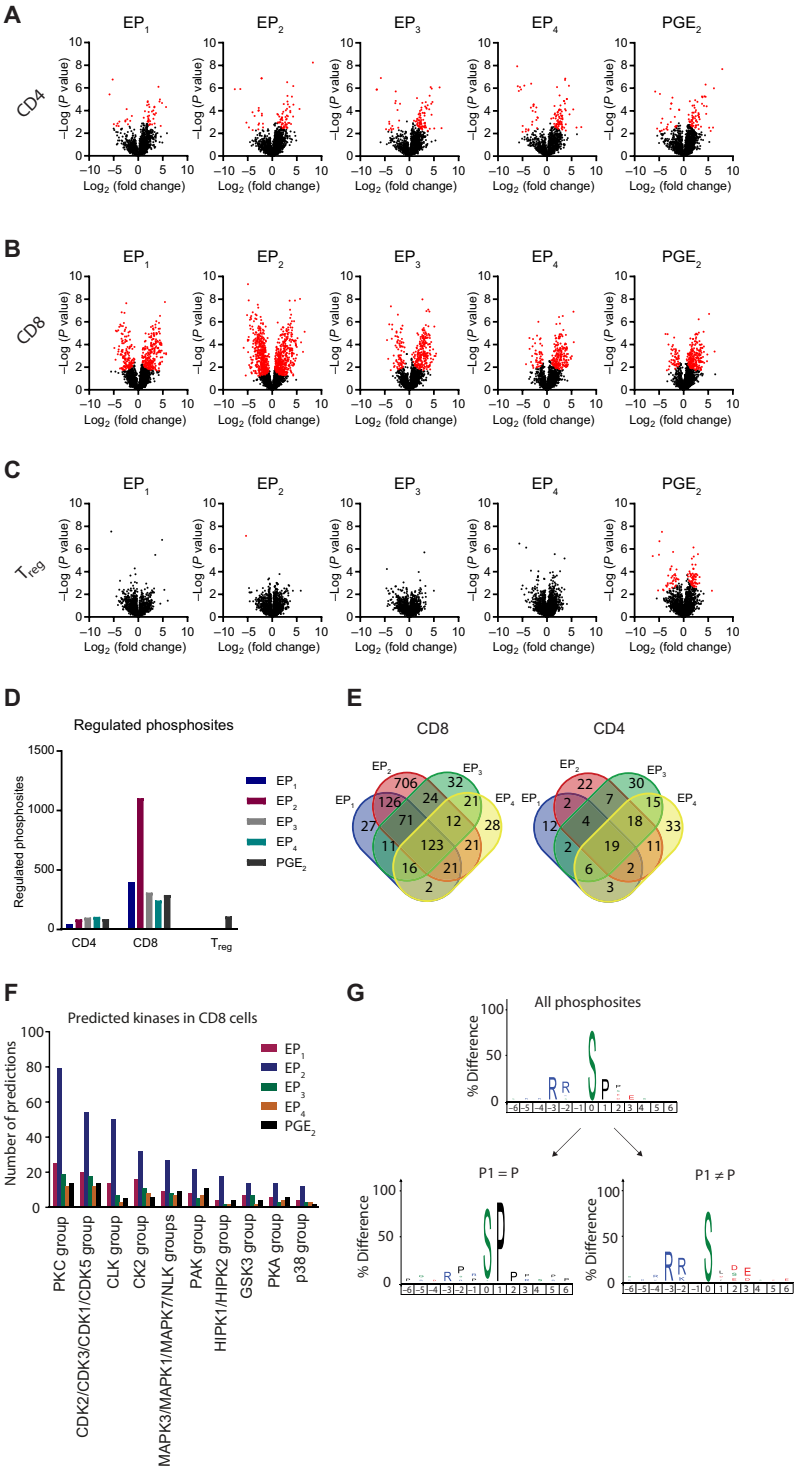

Fig. 1. Phosphoproteomic analysis reveals regulation of phosphosites by PGE_2 receptors in T cells. (**A** to **C**) Significantly regulated phosphoproteins in $CD4^+$ (A), $CD8^+$ (B), and T_{reg} (C) cells stimulated with 1 μM EP_1 agonist (ONO-DI-004; 2.5× EC_{50}), 0.04 μM EP_2 agonist (ONO-AE1-259-01; 10× EC_{50}), 0.05 μM EP_3 agonist (ONO-AE-248; 10× EC_{50}), 0.052 μM EP_4 agonist (ONO-AE1-329; 10× EC_{50}), 10 μM PGE_2, or vehicle. Significantly regulated phosphosites (two-way *t* test, S0 = 0.1, FDR = 5%) are shown in red. For each cell type, five healthy blood donors were used, providing five biological replicates. (**D**) Quantitation of regulated phosphosites under the different stimulation conditions in different subtypes of primary T cells. (**E**) Venn diagrams showing unique and overlapping phosphosites regulated under different stimulation conditions in $CD4^+$ and $CD8^+$ cells. (**F**) Groups of kinases regulating the observed changing phosphosites in $CD8^+$ cells were predicted using NetPhorest. (**G**) IceLogos showing the phosphorylation motifs that were most increased for the $CD8^+$ EP_2 stimulation condition. The IceLogo for all phosphosites that increased in abundance is shown above the IceLogos for those sites with (=) or without (≠) proline (P) in the P1 position.

$EP_{1–4}$ regulate different biological functions

Next, we used the "Predict Functional Phosphosites" (PFP) (*61*) tool to identify regulated phosphosites with a known biological function according to the PhosphoSitePlus database (Table 1) and sites predicted to be biologically relevant by at least one of the four algorithms in the program (table S3). Of the sites with known biological function, many are involved in signaling, and several are related to the kinases predicted above. For instance, we saw regulation of sites on Ca^{2+}/calmodulin-dependent protein kinase 2 (CAMK2), CDK9, p21-activated kinase 1 (PAK1), MAP3K5, PKC θ (PRKCQ), protein kinase D2 (PRKD2), ribosomal protein S6 kinase A3 (RPS6KA3), S6 ribosomal protein (S6RP), rapidly accelerated fibrosarcoma 1 (RAF1), and regulator of G protein signaling 3 (RGS3). Further, we observed many PKA-related regulated sites, for instance, PKA regulatory subunit RIα (PRKAR1A) Ser^{77} and Ser^{83}, protein tyrosine phosphatase nonreceptor type 7 (PTPN7) Ser^{44}, vasodilator-stimulated phosphoprotein (VASP) Ser^{239}, and vimentin (VIM) Ser^{26} and Ser^{73}. Many of the regulated sites are also particularly interesting in a T cell context, for instance, Ser^{697} and Ser^{706} of CD44, Tyr^{420} of the kinase FYN, Tyr^{394} and Tyr^{505} of the kinase LCK, and Tyr^{317} of phosphoprotein associated with glycosphingolipid-enriched microdomains 1 (PAG1).

Cellular functions regulated by the EPs

To further understand the range of biological processes regulated by the four PGE_2 receptors in T cells, the ClueGO software was used to analyze the regulated proteins for involvement in cellular functions (Fig. 2A, fig. S8, and table S4). In $CD4^+$ T cells and T_{regs}, no significant Gene Ontology (GO) term was enriched, whereas for $CD8^+$ T cells, all stimulation conditions showed enrichment for regulation of cytoskeleton organization, mRNA processing, cell-cell adhesion, cell polarity, and small guanosine triphosphatase (GTPase)–mediated signal transduction. Proteins involved in these various processes were also present in the list of biologically active phosphosites (Table 1 and table S3). For instance, several proteins related to small GTPase-mediated signal transduction—such as Rho guanine nucleotide exchange factors (ARHGEFs) 2, 6, and 7; β-arrestin 1; nuclear receptor coactivator 3; Rab GTPase-binding effector protein 1; RAF1; RGS3; and tripartite motif–containing 28—were observed among the regulated biologically active sites (Table 1 and table S3).

Table 1. Table of regulated phosphosites predicted to be functional. The Predict Functional Phosphosites (PFP) tool (www.kiharalab.org/web/pfp.php) was used to predict which of the regulated phosphosites identified in the current study are likely to be functional. The table shows regulated phosphosites that have known functions according to the PhosphoSitePlus database (actual class positive in PFP); most are also predicted to be functional by one of the four algorithms used by PFP. For a full overview of all regulated phosphosites predicted to be functional by at least one of the four algorithms in PFP or that are known to be functional according to the PhosphoSitePlus database, see the Supplementary Materials (table S2). Bold font indicates that the indicated phosphosite increases in abundance in response to stimulation. Regular font indicates that the abundance decreases in response to stimulation.

Phosphosite	EP_1	EP_2	EP_3	EP_4	PGE_2
ABI1 S183	**CD8**	**CD8**	**CD8**	**CD8**	**CD8**
ARHGEF2 S886		**CD8**			
ARHGEF6 S225		CD8			
ARHGEF6 S488	**CD8**	**CD8**	**CD8**	**CD8**	**CD8**
ARHGEF7 S518	**CD8**	**CD8**	**CD8**	**CD8**	**CD8**
ARRB1 S412	**CD8**	**CD8**	**CD8**	**CD8**	**CD8**
ATXN1 S775		CD8			
BAD S118	CD8	CD8			
BANF1 S4	**CD8**	**CD8**	**CD8**	**CD8**	**CD8**
BANF1 T2	**CD8**	**CD8**	**CD8**	**CD8**	**CD8**
BANF1 T3	**CD8**	**CD8**	**CD8**	**CD8**	**CD8**
BTG1 S159		**CD8**			
CAD S1406		**CD8**			**CD8**, **T_{reg}**
CALM2 S82	**CD8**	**CD8**	**CD8**		**CD8**
CAMKK1 S458	**CD8**	**CD8**			
CARHSP1 S41		**CD8**			
CBL S619		**CD8**			
CD247 Y123	**CD8**	**CD8**	**CD8**		
CD44 S697					**T_{reg}**
CD44 S706	**CD8**	**CD8**	**CD8**	**CD8**	
CDK9 S347		CD8			
CREB1 S271		**CD8**			
DAP S3		CD8			
DBN1 S142		CD8			
DBNL S269	CD8	CD8	CD8		
DBNL T291		**CD8**			
DCK S11	CD8				**CD8**
DNM1L S616		**CD8**	**CD8**		
DSN1 S109		**CD8**			**CD4**, **T_{reg}**
EEF1D S133	CD8	CD8	CD8		
EEF2 T57		CD8			
EIF2S2 S2	**CD8**	**CD8**	**CD8**	**CD8**	**CD8**
ETS1 S282				**CD4**	
FAM129A S602		**CD8**			
FLNA S1459	**CD8**	**CD8**	**CD8**	**CD8**	**CD8**
FLNA S2152		**CD8**			
FOXO1 S287		**CD4**			
FYN Y420		CD8			
G3BP1 S149				CD8	
HDAC7 S486		**CD8**			

continued to next page

Phosphosite	EP_1	EP_2	EP_3	EP_4	PGE_2
HMGN1 S7		CD8			
HNRNPK S284			**CD8**		
ITPR1 S1598		CD8			
KIF3A S687					**T_{reg}**
KLC2 S582		**CD8**			
LASP1 S146	CD4				
LCK Y394		CD8			
LCK Y505	**CD4**	**CD4**	**CD4**	**CD4**	**CD4**
LCP1 S5	CD8	CD8	CD8	CD8	**CD4**
LIG1 S66		**CD8**			**CD8**
LMNA S390		**CD8**			
LSP1 S252	CD8	CD8	CD8		
MAP3K5 S1033	**CD4**		**CD4**	**CD4**	**CD4**
MCM2 S27		CD8			
MVB12A S170		**CD8**	**CD8**		
MYH9 S1943		CD8			
NCOA2 S493	CD8	CD8			
NCOA3 S857		**CD8**			
NDRG1 S330		CD8			
NF2 S518	**CD8**	**CD8**	**CD8**	**CD8**	**CD8**
NIFK T238					T_{reg}
NOP58 S502		**CD8**			
NPM1 S10		**CD8**			
PAG1 Y317				**CD8**	**CD8**
PAK1 S174			CD8		
PDHA1 S293	**CD8**	CD8	CD8	CD8	
PEA15 S104		CD8			
PEA15 S116		**CD8**			
PFKFB3 S461		CD4		CD4	
PIKFYVE S307		**CD8**			
PKN2 T958			**CD8**	**CD8**	
PPP1R12A S445			CD8		CD8
PPP1R12A T696		**CD8**			
PPP2R5A S41		**CD8**			
PRKAR1A S77		**CD8**			
PRKAR1A S83		**CD8**			
PRKCQ S676	**CD8**	**CD8**			
PRKCQ S695		**CD8**			
PRKCQ T538			CD8		
PRKD2 S710				**CD4**	
PTPN7 S44	CD8			CD8	CD8
RABEP1 S407	CD8	CD8			
RAF1 S43		CD8			
RBBP8 S327					**T_{reg}**
RBL2 S1080					T_{reg}

continued to next page

Phosphosite	EP_1	EP_2	EP_3	EP_4	PGE_2
RGS3 S943		**CD8**			
RPS6 S235					**CD8**, **T_{reg}**
RPS6 S236					**CD8**, **T_{reg}**
RPS6KA3 S227		**CD8**	**CD8**	**CD8**	**CD8**
SAMSN1 S23		**CD8**			
SH3KBP1 S587					CD4
SLAMF6 Y309		**CD8**			
SMN1 S28				**CD4**	
SSB S366		CD8			
STAT1 S727		**CD8**	**CD8**	**CD8**	**CD8**
STAT5A S780		**CD8**	**CD8**		CD8
STIM1 S608					T_{reg}
TACC3 S558					**CD8**
TNIK S764		**CD8**			
TRIM28 S473	CD8	CD8	CD8		
USP20 S333					**T_{reg}**
VASP S239					**CD8**
VIM S26	**CD8**		**CD8**	**CD8**	**CD8**
VIM S73		CD8			
ZC3HC1 S395	CD8	CD8		CD8	

As expected, several immune processes were also highly predicted by ClueGO (Fig. 2B, fig. S9, and table S5). For EP_2, the most highly predicted immune process was TCR signaling, which corroborated previous findings that EP_2 inhibits TCR signaling (*1*). This process was also highly enriched in PGE_2-stimulated $CD8^+$ cells. Other highly enriched immune processes included T cell activation (for EP_1, EP_3, and PGE_2), establishment of T cell polarity (EP_3, EP_4, and PGE_2), thymic T cell selection and T cell differentiation in thymus (EP_1, EP_3, and EP_4), lymphocyte migration (EP_4), and lymphocyte proliferation (EP_3).

Receptor- and cell type–specific regulation of phosphosites

The specific signaling elicited through each receptor was examined in more detail using an approach that combines fluorescent cell barcoding with phosphoflow cytometry (*62*). This technique allows for high-throughput monitoring of phosphorylation events resulting from a given stimulus or combination of stimuli, yielding information on signaling kinetics, magnitudes, and differences across T cell subtypes. A panel of 16 phospho-specific antibodies was established on the basis of known PGE_2 signaling pathways in T cells as well as the current phosphoproteomics study. The signaling elicited by specific agonists of each of the four EPs was monitored over time in $CD4^+$ and $CD8^+$ naïve ($CD45RA^+$) and effector/memory ($CD45RO^+$) T cells (Fig. 3, A and B; and figs. S10, S11, S12, A to C, and S13, A to C).

Many readouts in the phosphoflow cytometry panel, including glycogen synthase kinase 3 α (GSK3A) $pSer^{21}$ (*63*), VASP $pSer^{157}$ (*64*), VIM $pSer^{38}$ (*65*), histone H3 $pSer^{10}$ (*66*), cAMP response element–binding protein 1 (CREB1) $pSer^{133}$ (*67*), and heat shock protein B1 (HSPB1) $pSer^{78}$ (*68*), can be directly phosphorylated by PKA, which is activated immediately downstream of EP_2 and EP_4, following $G_{\alpha s}$ activation and cAMP production by adenylyl cyclase. As expected, the abundance of these phosphorylated PKA substrates was strongly increased by EP_2 or EP_4 agonist stimulation. A further three phosphoflow readouts were phosphosites on different subunits of PKA [PRKAR2A ($pSer^{99}$), PRKAR2B RIIb ($pSer^{114}$), and PRKACA ($pThr^{197}$)], of which the first two are thought to be autophosphorylated (*69*, *70*), and the latter is an activating site that appears to be phosphorylated by phosphoinositide-dependent kinase 1 (PDK1) in vivo (*71*, *72*). Counterintuitively, these three phosphosites demonstrated decreased abundance upon treatment with EP_2 or EP_4 agonists, although this observed reduction is likely due to postactivation desensitization.

Of the remaining monitored sites, several can be downstream of PI3K-Akt pathways, which, in turn, can be activated by $G_{\beta\gamma}$ signaling (*73*–*75*) and β-arrestin signaling (*76*, *77*). In particular, the EP_4 receptor, when coupled to $G_{\alpha i}$, is known to trigger a PI3K pathway through $G_{\beta\gamma}$ signaling (*28*). Potential PI3K-Akt–regulated phosphoflow readouts included N-Myc downstream regulated 1 (NDRG1) $pThr^{346}$, which can be phosphorylated by serum and glucocorticoid–regulated kinase 1 (SGK1) downstream of PI3K (*78*) or by Akt downstream of CD28 (*79*), as well as S6RP ($pSer^{240}$), which can be phosphorylated by ribosomal protein S6 kinase (p70S6K) downstream of PI3K and mechanistic target of rapamycin (*80*). The other monitored phosphosite on S6RP, $pSer^{235/236}$, is thought to be phosphorylated by a different kinase, namely, p90S6K, operating downstream of ERK (*80*). In agreement with previous studies (*80*), distinct kinetics were observed for the two phosphorylation events on S6RP, with the Ser^{240} phosphorylation site displaying a slower response than $Ser^{235/236}$, suggesting that two different kinases with different kinetics are operating in T cells as well.

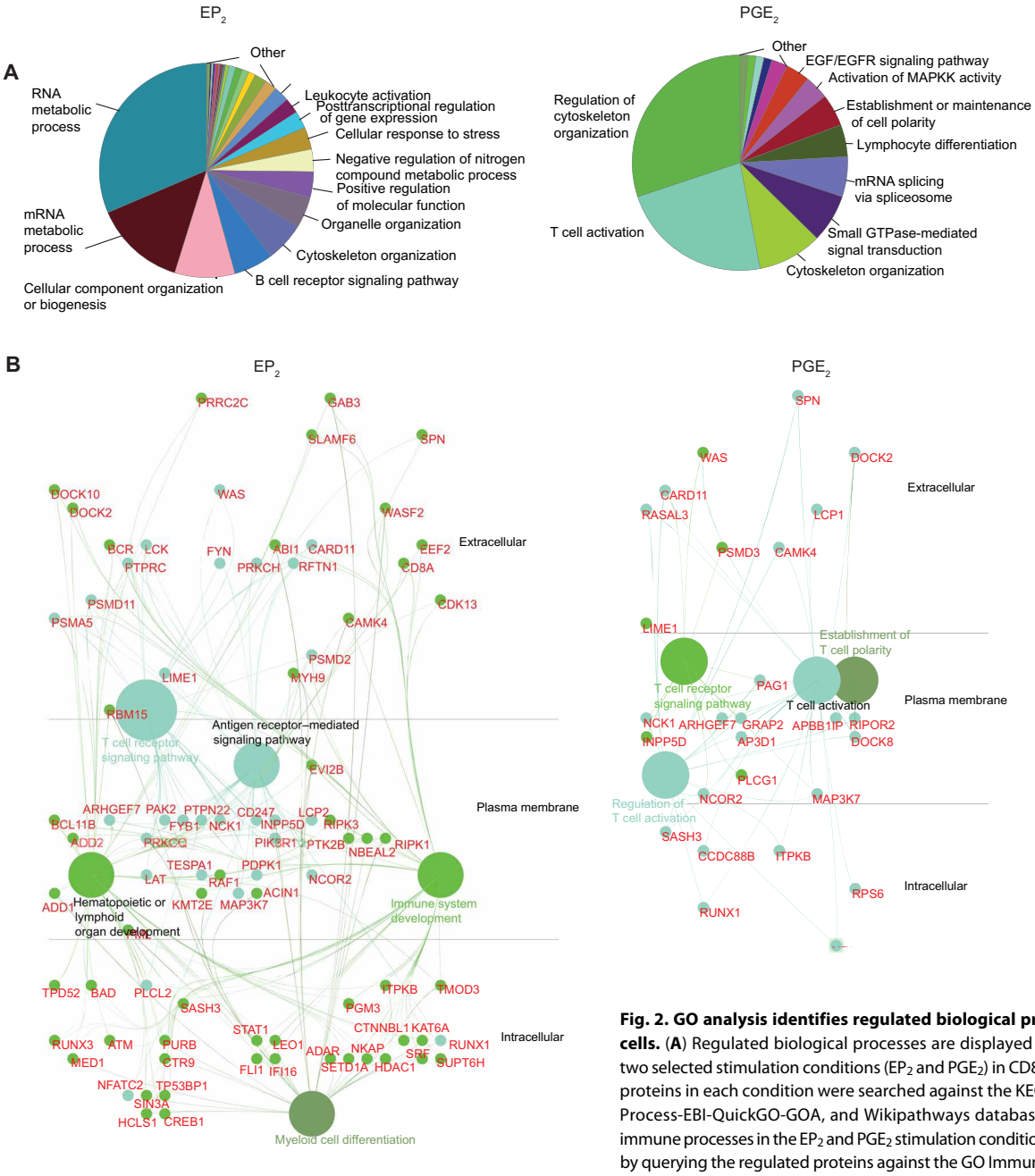

Fig. 2. GO analysis identifies regulated biological processes in CD8$^+$ cells. (**A**) Regulated biological processes are displayed as a pie chart for two selected stimulation conditions (EP_2 and PGE_2) in CD8$^+$ cells. Regulated proteins in each condition were searched against the KEGG, GO Biological Process-EBI-QuickGO-GOA, and Wikipathways databases. (**B**) Regulated immune processes in the EP_2 and PGE_2 stimulation conditions were identified by querying the regulated proteins against the GO ImmuneSystemProcess-EBI-QuickGO-GOA database. Regulated biological processes and pathways and associated regulated proteins are displayed in cerebral (cell region–based rendering and layout) format, which superimposes the interaction network on the subcellular locations of the components.

The two final phosphoflow readouts, PLC γ1 (PLCG1) pTyr^{783} and histone H3 pSer^{28}, have several potential regulatory kinases, but it is thought that PLCG1 phosphorylation at Tyr^{783} is downstream of TCR activation (*81*, *82*) and that histone H3 pSer^{28} is phosphorylated by Aurora B kinase, mitogen- and stress-activated protein kinase 1 and 2 (*66*), or MAPKs (*83*). Many of the readouts discussed above as PKA or Akt substrates may also be phosphorylated by other kinases, depending on context.

Overall, the monitored phosphoflow readouts responded most strongly to EP_2 and EP_4 agonist stimulation, with smaller or sometimes absent responses to EP_1 and EP_3. Control stimulation with PGE_2, as expected, led to a robust response for all readouts. The addition of receptor antagonists reversed the signaling elicited by the agonists (fig. S14). The strong responses to EP_4 and, especially, EP_2 agonist stimulation may be due to the higher abundances of EP_2 and EP_4 than of EP_1 and EP_3 in peripheral blood T cells (*26*), although all appear to be present (fig. S1) (*25*).

The kinetics of phosphorylation events varied considerably between readouts in this study, with some showing early (VIM pSer^{38} and VASP pSer^{157}), medium (S6RP pSer^{240} and NDRG1 pThr^{346}),

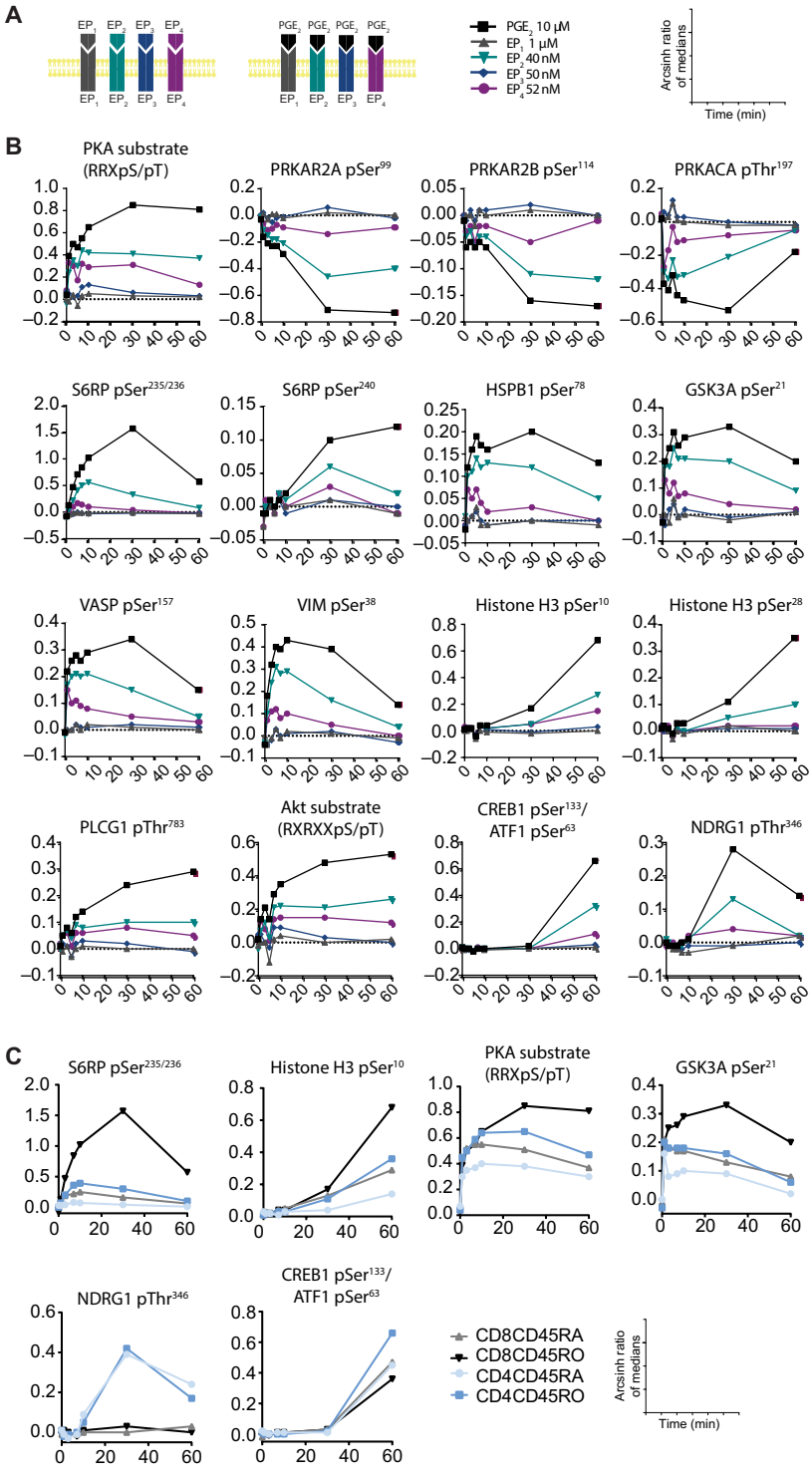

Fig. 3. Phosphoflow cytometry demonstrates receptor- and cell type–specific regulation of a panel of markers. (**A**) Schematic of the stimulation setup and graph key. (**B**) Time courses of the regulation of the 16 indicated phosphopeptides monitored by phosphoflow after stimulation. Cells were stimulated with either a single receptor-specific agonist or PGE_2, which targets all four receptors. The agonists used were 1 µM ONO-DI-004 (EP_1), 0.04 µM ONO-AE1-259-01 (EP_2), 0.05 µM ONO-AE-248 (EP_3), and 0.052 µM ONO-AE1-329 (EP_4); and PGE_2 was used at 10 µM. The symbol and color-coding key and graph axis labeling apply to all graphs in the panel. All readouts shown are from $CD8^+CD45RO^+$ cells, except CREB ($pSer^{133}$) and NDRG ($pThr^{346}$), which are from $CD4^+CD45RO^+$ cells. (**C**) Time course for the regulation of the indicated phosphopeptides in $CD8^+CD45RA^+$, $CD8^+CD45RO^+$, $CD4^+CD45RA^+$, and $CD4^+CD45RO^+$ cells stimulated with PGE_2. Cells were stimulated with 1 µM PGE_2, except for NDRG1 $pThr^{346}$, where stimulation was carried out with 10 µM PGE_2. Data shown are for one representative experiment; two replicates are included in the Supplementary Materials (figs. S12 and S13).

or late (CREB1 $pSer^{133}$ and histone H3 $pSer^{10}$ and $pSer^{28}$) phosphorylation responses (Fig. 3, A and B). One explanation for this observation could be that it reflects different cellular locations. For instance, CREB1 and histone H3, which exhibited slow temporal regulation, are both located in the nucleus, whereas the early and medium readouts listed above are cytoplasmic. Different signaling pathways may also have different dynamics independent of location, for instance, in the case of S6RP phosphorylation by two different kinases as described above. The difference in timing may, in some cases, also stem from differences between G protein–dependent (G_α and $G_{\beta\gamma}$) signaling, which tends to occur relatively rapidly (*84*, *85*), and G protein–independent (β-arrestin) (*35*, *36*) signaling, although the latter may, in some cases, also proceed quickly (*86*).

The phosphoflow cytometry approach further revealed considerable differences in PGE_2-induced signaling between T cell subtypes (Fig. 3C). In particular, for the vast majority of the readouts, the signals were the strongest and most persistent in $CD8^+CD45RO^+$ cells. S6RP $pSer^{235/236}$, GSK3A $pSer^{21}$, PKA substrates, and histone H3 $pSer^{10}$ were examples of this (Fig. 3C). In a few cases, however, the highest amounts of signaling were observed in $CD4^+$ cells, for instance, for NDRG1 ($pThr^{346}$) and CREB1 ($pSer^{133}$). These cell type–specific differences in PGE_2 signaling in T cells may reflect differences in the abundances of individual EPs or distinct downstream signaling pathways in different cell types.

EP_2 and EP_4 regulate phosphosites with different kinetics

EP_2 and EP_4 both couple to $G_{\alpha s}$ and might thus be expected to signal through many of the same downstream pathways. Agonists of these receptors triggered the same readouts in our phosphoflow panel (Fig. 3, A and B). However, it was notable that the signals triggered by EP_2 were substantially stronger than those from EP_4 and also persisted longer (Fig. 4A and fig. S15, A and B). To confirm that this was not an effect of different doses, potencies, or other properties of the receptor agonists, we performed an experiment to isolate PGE_2 signaling through a specific receptor by stimulating $CD3^+$ cells with PGE_2 while simultaneously blocking three of the four EP receptors with specific antagonists (Fig. 4, B and C). Using this approach, we confirmed that the same concentration of PGE_2 gave a stronger signaling response through EP_2 than through

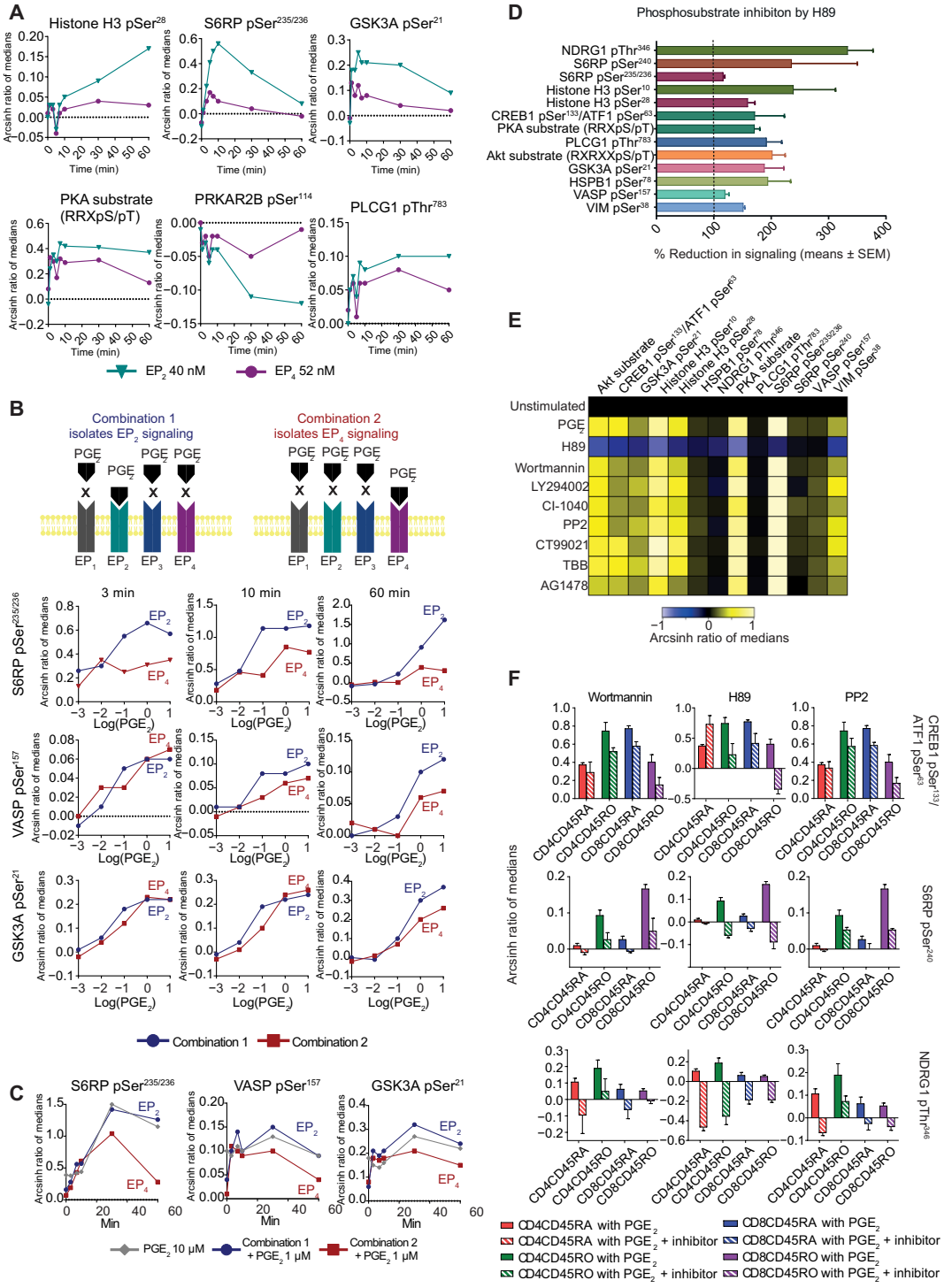

Fig. 4. Signaling differences between EP_2 and EP_4 receptors and effects of kinase inhibitors. (**A**) Comparison of intensity and duration of signaling through EP_2 (40 nM ONO-AE1-259-01) and EP_4 (52 nM ONO-AE1-329) receptors in $CD8^+CD45RO^+$ cells. Data shown are from one representative experiment; replicates are included in the Supplementary Materials (figs. S12 and S13). (**B**) $CD3^+$ cells were stimulated with different concentrations of PGE_2 in combination with antagonists to isolate PGE_2 signaling through either EP_2 (combination 1) or EP_4 (combination 2). The graphs show the degree of phosphorylation of the indicated phosphosites relative to the concentration of PGE_2 in $CD8^+CD45RO^+$ cells. Key findings were repeated with $n = 3$ (fig. S15). (**C**) Time course of the abundances of the indicated phosphosites in $CD8^+CD45RO^+$ cells stimulated with combination 1 + PGE_2, combination 2 + PGE_2, or PGE_2 alone. (**D**) Inhibition of the phosphorylation of the 13 indicated phosphosites downstream of PGE_2 by the PKA inhibitor H89. Percent inhibition was calculated relative to 10 μM PGE_2 stimulation, and phosphorylation responses are shown at 10 min, except for NDRG1 $pThr^{346}$ (30 min), S6RP $pSer^{240}$ (30 min), histone H3 $pSer^{10}$, $pSer^{28}$ (60 min), and CREB1 $pSer^{133}$/ATF1 $pSer^{63}$ (60 min). Responses were measured in $CD8^+CD45RO^+$ cells, except for NDRG1, which was measured in $CD4^+CD45RO^+$ cells. Data are means + SEM, $n = 3$. (**E**) Heatmap showing inhibition of phosphosites after 60 min of stimulation with PGE_2 in the presence of inhibitors in $CD8^+CD45RO^+$ cells. Signals were calculated relative to the unstimulated control. Data are representative of three independent experiments. (**F**) Phosphorylation of NDRG1 (30 min), S6RP (30 min), and CREB1 (60 min) in the indicated cell types in the presence of Wortmannin, H89, or PP2. Date are means ± SEM, $n = 3$. Samples were normalized to the unstimulated sample.

EP_4 (Fig. 4B). The signaling intensity of EP_2-isolated PGE_2 signaling, EP_4-isolated PGE_2 signaling, and PGE_2 signaling through all four receptors was then compared over time (Fig. 4C). The experiment confirmed the observation from the agonist-based studies that EP_2 signaling had longer duration and higher intensity than EP_4 signaling, independently of any specific agonist properties. In general, PGE_2 signaling through EP_2 produced a signal equivalent to PGE_2 signaling through all four receptors, in some cases exceeding it, whereas EP_4 signaling was less intense. The observation that EP_2-isolated PGE_2 signaling sometimes produced slightly higher phosphoflow responses than PGE_2 signaling through all receptors could possibly be due to PGE_2-induced $G_{\alpha i}$ activation through, for instance, EP_3 and EP_4, which could temper $G_{\alpha s}$ signaling through EP_2 when all receptors are stimulated simultaneously.

Phosphoflow cytometry inhibitor studies

To further investigate which kinases are involved in the PGE_2 signaling pathways in T cells, phosphoflow cytometry was applied in the presence of PGE_2 stimulation and various kinase inhibitors. First, we observed that PGE_2 regulation of all monitored readouts was inhibited by at least 100% by the PKA inhibitor H89 (Fig. 4D). Here, we defined 100% inhibition as a reduction in the phosphorylation of a given readout to the amount observed in the unstimulated sample. Any inhibition beyond 100% thus constitutes a reduction in the basal phosphorylation of these phosphosites. Several readouts were inhibited by 200% or more (Fig. 4D), indicating considerable basal PKA signaling in the absence of PGE_2 stimulation. Most of the sites regulated by PGE_2 in T cells thus appear to be downstream of PKA, in line with the observation that the phosphoflow readouts were mainly affected by signaling through the EP_2 and EP_4 receptors, which are known to couple to $G_{\alpha s}$ and PKA.

In addition to H89, inhibitors of other important kinases in T cells, including PP2 (Src inhibitor), Wortmannin (PI3K inhibitor), LY294002 (PI3K inhibitor), CI-1040 [mitogen-activated protein kinase kinase (MEK) inhibitor], AG1478 [epidermal growth factor receptor (EGFR) inhibitor], TBB (CK2 inhibitor), and CT99021 (GSK3A and GSK3B inhibitor), were also tested (Fig. 4E). Although H89 generally gave the strongest inhibitory response, some readouts were also inhibited by other kinase inhibitors, indicating that these phosphosites are downstream of signaling pathway(s) involving several different kinases.

For instance, NDRG1 $pThr^{346}$ was inhibited by Wortmannin, LY294002, and PP2 in addition to H89, indicating regulation by PI3K and Src. S6RP $pSer^{240}$ was also inhibited by these inhibitors, as well as by CT99021 and TBB, suggesting that this phosphosite is downstream of several different pathways, also involving GSK3A/B and CK2. CREB1 $pSer^{133}$ was a further readout influenced by several inhibitors—most strongly by H89, Wortmannin, LY294002, CI-1040, and PP2. This is in line with the literature, in which CREB1 $pSer^{133}$ has been reported to be downstream of several pathways and kinases including PKA, PI3K-Akt, and PKC (*67*, *87*).

Considerable cell type differences were observed in these inhibitor studies (Fig. 4F and fig. S16). For CREB1 $pSer^{133}$, there was a notable difference between the cell types in that Wortmannin, H89, and PP2 inhibited this readout substantially except in $CD4^+CD45RA^+$ cells. Another readout that exhibited a cell type–specific inhibition pattern was NDRG1 $pThr^{346}$. This phosphosite was inhibited to below baseline by Wortmannin, H89, and PP2 in $CD4^+CD45RA^+$ cells, but only by H89 in $CD4^+CD45RO^+$ cells, indicating that there may be basal signaling through all three kinases in $CD4^+CD45RA^+$ cells but only through PKA in $CD4^+CD45RO^+$ cells. S6RP $pSer^{240}$ phosphorylation was also affected differently by inhibitors in different cell types. In particular, both Wortmannin and PP2 inhibited this phosphorylation to baseline or below in naïve ($CD45RA^+$) $CD4^+$ and $CD8^+$ cells but only by about 40 to 70% in effector/memory ($CD45RO^+$) $CD4^+$ and $CD8^+$ cells. Together, these results suggest that the contributions of different signaling pathways may differ considerably between cell types.

Overview of PGE_2 signaling in T cells by network modeling

Network modeling was used to obtain an estimate of PGE_2 signaling pathways activated in $CD4^+$ and $CD8^+$ T cells under separate and combined stimulation conditions. To this end, an Integer Linear Programming (ILP) formulation of PHOsphorylation NEtworks for Mass Spectrometry (PHONEMeS) (*88*) was applied by combining the large-scale phosphoproteomic dataset with a network of directed protein and kinase and phosphatase–to–substrate (K/P-S) interactions representing our prior knowledge. PHONEMeS identifies subnetworks that best explains the signal propagation resulting in the measured phosphoproteomic data for each of the experimental conditions. This allows us to extract possible paths connecting the stimulated receptors to the downstream regulated phosphosites. This approach yielded network models for each of the five different stimulation conditions and one network model when considering all the combined experimental conditions in $CD4^+$ (Fig. 5, A and B, and figs. S17A, S18A, S19A, S20A, S21A, and S22A) and $CD8^+$ (Fig. 5C and figs. S17B, S18B, S19B, S20B, S21B, and S22B) T cells. Modeling was not performed in T_{regs}, due to the low number of regulated phosphosites in this cell type, which did not permit robust analysis.

The modeled networks provided an overview of possible signaling networks through all receptors in both cell types in PGE_2-stimulated conditions and, when signaling through specific receptors, were isolated by stimulating cells with PGE_2 in combination with three receptor-specific antagonists (Fig. 5A and figs. S21 and S22). From the modeled networks, it appeared that the same main pathways were active in $CD4^+$ and $CD8^+$ cells for a given stimulation condition. For instance, for EP_2, the main signaling appeared to proceed through PKA, Src, GSK3, CK2, and MAPK-based pathways in both cell types (Fig. 5, B and C, and fig. S18). This was in line with results from the phosphoflow cytometry study, which also suggested that the difference in signaling between cell types may be more one of strength and duration of signaling rather than different pathways, with a few notable exceptions (Fig. 4F). In the phosphoproteomics results, strength of signaling appeared to translate into a larger number of observed readouts, resulting in a larger predicted network for $CD8^+$ than for $CD4^+$ cells, although essentially centered on the same key pathways, indicating most of the preserved pathways between cell types.

Modeled networks for the different stimulation conditions successfully recapitulated the main expected pathways, including PKA-based pathways for EP_2 and EP_4 and PKC-based pathways for EP_1. A good correspondence was also observed between the predicted networks and NetPhorest-predicted kinases (Fig. 1F and table S2) and kinases implicated based on inhibitor studies (Fig. 4E). In particular, the key kinases identified in the inhibitor studies, such as PKA, Src, and PI3K, were prominently present in the predicted networks for most stimulation conditions. The five most highly predicted kinase groups by NetPhorest, including PKC, CDKs, CLKs, CK2, and MAPK, were also present in the predicted networks. CLKs were only present in a few predicted networks, notably EP_1 and EP_2 signaling in $CD8^+$ cells, but these were the most highly predicted conditions for CLKs by NetPhorest as well. We noted that G protein–independent pathways were highly predicted in the networks. In particular, β-arrestin accounted for a substantial part of the signaling in all stimulation conditions, according to the predicted networks. Although it is known that PGE_2 can signal through β-arrestin–mediated pathways, the extent of the predicted contribution was greater than expected.

DISCUSSION

Phosphoproteomics of T lymphocytes

MS-based phosphoproteomics has undergone major developments in recent years, allowing the detection of ever-increasing numbers of phosphosites in only a few hours (*89*). In T cells, a few phosphoproteomics studies have investigated signaling, including that induced

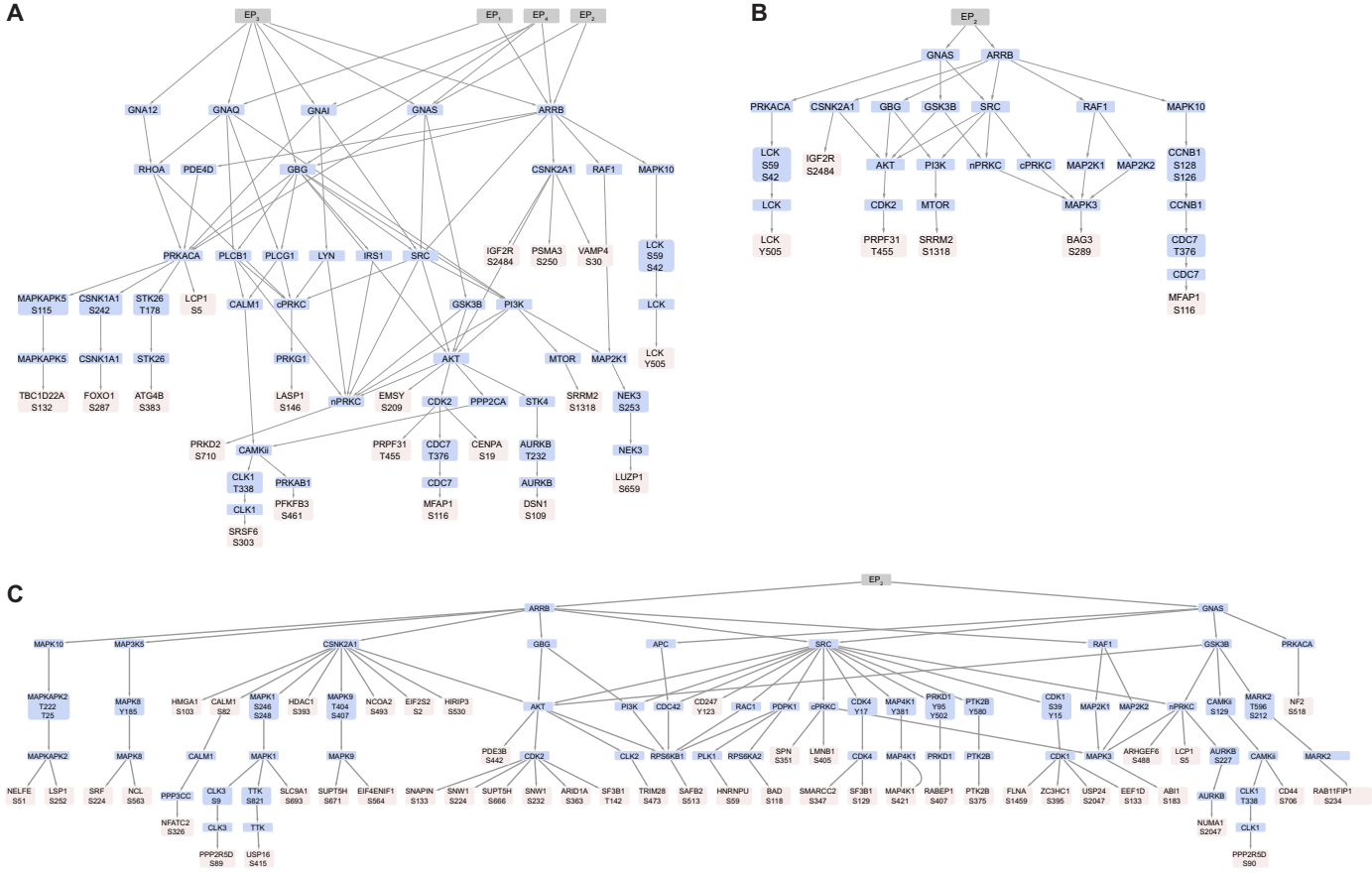

Fig. 5. Signaling networks for different stimulation conditions modeled using PHONEMeS. (**A** to **C**) Phosphosites observed to be regulated by phosphoproteomics were used as input for the PHONEMeS algorithm, which maps this information onto a background network constructed from known K/P-S and protein-protein interactions. PHONEMeS then optimizes the network and extracts possible paths connecting the stimulated receptors with the perturbed phosphosites by using an Integer Linear Programming (ILP) formulation and lastly evaluates the network by comparison with the data. This approach yielded network models of each of the five different stimulation conditions in $CD4^+$ and $CD8^+$ cells. Shown here are the modeled networks for the combined results of stimulation with the four different receptor agonists in $CD4^+$ cells (A) and stimulation with only the EP_2 agonist in $CD4^+$ cells (B) and $CD8^+$ cells (C).

by PGE_2 (*53*–*55*, *90*, *91*). Here, our mapping of phosphoproteome changes in individual PGE_2 signaling pathways in three primary T cell subsets—helper T cells ($CD4^+$), cytotoxic T cells ($CD8^+$), and T_{regs}—through each of the four PGE_2 receptors identified more than 12,500 phosphopeptides and quantified changes in 5000 to 8000 phosphosites, which is comparable coverage to that in related studies (*55*).

Kinase nodes in PGE_2 signaling

The kinases predicted here show substantial overlap with previous studies and support the finding that PKA, CAMK2, Akt, GSK3, and CK2 are major contributors to PGE_2 signaling in T cells (*53*, *55*). PKA is not as highly predicted as in previous studies (*53*), which could be due to the overlapping substrate motifs of PKA, PKC, and protein kinase B (Akt) (*92*). Inhibitor phosphoflow cytometry experiments certainly support a key role for PKA in PGE_2 signaling, although with the caveat that H89 is known to have some cross-reactivity with other kinases (*93*, *94*). When combined with cAMP stimulation, however, H89 is quite specific for PKA.

Kinase contributions differed across T cell subtypes. For instance, CK2 was more highly predicted in $CD4^+$ than in $CD8^+$ cells. Regulated phosphomotifs exhibited similar cell type differences, with $CD4^+$ cells having a greater proportion of acidophilic, potential CK2 target motifs and a lower proportion of basophilic, potential PKA, PKC, PKG, Akt, p70 S6 kinase, AMPK, and RSK target motifs than $CD8^+$ cells. CK2 is thought to predominantly have a proinflammatory role in T cells (*95*–*98*), although its role in different subsets is not well understood. It is notable that PGE_2 may be one of the factors regulating CK2 activity through a positive feedback loop. Overall, the high degree of conservation of EP-activated kinases between T cell subtypes likely indicates that PGE_2 has largely shared functions in different T cell subtypes. However, there appear to be some interesting exceptions, for instance, CK2, where PGE_2 may signal through distinct pathways and distinct kinase nodes depending on cell type, leading to distinct PGE_2 functional output between cell types as well.

Tyrosine-centered phosphorylation motifs

Only about 2% of identified phosphosites by IMAC-based MS studies are tyrosine-centered (*90*), and a low abundance of these sites was observed in the current study as well. A few tyrosine phosphosites were, however, regulated. Phosphorylation of the inhibitory Tyr^{505} site on LCK was found to be increased in all stimulation conditions

in $CD4^+$ cells, perhaps indicating that the inhibitory pathway involving phosphorylation of this site is more active in $CD4^+$ than in $CD8^+$ cells (*42*). Further, phosphorylation of the activating site on Src or Fyn (Tyr^{419} or Tyr^{420}, respectively) was decreased upon EP_2 stimulation, in line with the previous observation that cAMP-PKA signaling reduces Src activity (*99*). On the other hand, phosphoflow cytometry studies with inhibitors (Fig. 4, B to F) suggested the activation of Src, as did network modeling, perhaps indicating transient activation.

Predicting functions of PGE_2 in T cells

Now, a general problem in phosphoproteomics studies is that most phosphosites detected have no known biological function, making functional assignments challenging (*92*). However, using function prediction analysis of PGE_2-regulated phosphosites, it was possible to identify some sites with known or predicted biological function (Table 1 and table S3), and GO analysis further implicated PGE_2-regulated species in key cellular and immunological processes (Fig. 2). One of the most highly predicted processes in all stimulation conditions was cytoskeleton remodeling, which agrees with findings in other cell types (*56*), and may be mediated partly by PKA through phosphorylation of proteins involved in cytoskeletal processes, such as VASP Ser^{157}, Ser^{239}, and Thr^{278} (*100*); VIM Ser^{38} (*65*); or HSPB1 Ser^{78} (Fig 4). Processes related to RNA processing, including transcription, were also highly predicted (Fig. 2), in line with the observed regulation of several transcription-related outputs histone H3 and CREB1) by phosphoflow cytometry, indicating that PGE_2 may also be important in regulating RNA-related cellular functions. PGE_2 signaling through the four EPs was also implicated in regulating several important immune-specific functions such as T cell proliferation (Fig. 2B), which agrees with a large literature (*27*, *101*, *102*). In addition, a number of the regulated phoshoflow cytometry readouts, notably Akt, NDRG, S6RP, and CREB1, are also involved in cell proliferation, further supporting a role for PGE_2 in regulating T cell proliferation. TCR signaling was predicted by GO analysis in the EP_2 and PGE_2 conditions, in line with a literature on the inhibition of TCR signaling by EP_2, and to some extent EP_4, by PGE_2 (*42*, *43*). Last, T cell activation was highly predicted in several conditions, as also seen in previous studies (*53*). Together, our results support a broad role for PGE_2 signaling through the four EP receptors in regulating important cellular and immunological functions in T cells.

Cell type and receptor differences in PGE_2 signaling

Some signaling pathways become only very transiently activated upon PGE_2 stimulation (*55*), necessitating the use of a dynamic profiling technique with high temporal resolution, such as multiplexed phosphoflow cytometry. Our phosphoflow panel consisted of 16 antibodies, recognizing phosphorylated proteins involved in a number of biological processes; ranging from translational regulation (S6RP) to cytoskeletal remodeling (VASP, VIM, and HSPB1), proliferation (NDRG1), and transcription (histone H3, CREB1); and echoing the functions predicted for PGE_2 in the GO analysis of regulated sites in the phosphoproteomics study.

The temporal profiles of EP_2 and EP_4 signaling differed markedly despite both receptors primarily coupling to $G_{\alpha s}$. The shorter signal duration of EP_4 could be due to more rapid receptor internalization (*103*). As for the differing signal intensity, EP_4 is thought to have weaker functional coupling to cAMP and PKA than EP_2 due to its ability to also couple to $G_{\alpha i}$ (*30*). Thus, stimulation of EP_2 by PGE_2 leads to higher cAMP amounts than equivalent stimulation of EP_4, assuming equal abundances of the receptors (*29*). EP_2 may be present in higher amounts than EP_4 in T cells (*26*). Thus, PKA-dependent readouts would be expected to change more strongly in response to EP_2 stimulation (*30*), as observed here. In addition, $G_{\alpha i}$ signaling is associated with concomitant $G_{\beta\gamma}$ release and signaling, and in the case of EP_4, $G_{\alpha i}$ coupling triggers a PI3K signaling pathway and inhibits PKA (*28*, *104*), possibly also contributing toward the observed lower signaling intensity for EP_4. We speculate that the differences in signaling intensity and kinetics between the EP_2 and EP_4 receptors may yield distinct cellular effects even though many of the sites regulated are shared between the two receptors.

Most phosphoflow cytometry readouts displayed the highest levels of signaling in CD8CD45RO cells, with a few readouts (notably NDRG1 and CREB1) showing the highest signaling levels in CD4 T cells. Inhibitor phosphoflow cytometry experiments echoed the findings from kinase predictions and motif analysis, namely, that whereas some kinases, such as PKA, contribute strongly in all cell types, other signaling pathways contribute differentially across T cell subtypes, highlighting the diversity and complexity of PGE_2 functions in the immune system.

Evidence for G protein–dependent PGE_2 signaling pathways from network modeling

The G_α-triggered pathways for the EP receptors were likely responsible for much of the signaling observed by MS and phosphoflow and were all recapitulated in the modeled networks. For instance, EP_2 and EP_4 signaling through $G_{\alpha s}$ and PKA-based pathways were present in the modeled networks both in $CD4^+$ and $CD8^+$ cells, and many PKA substrates were phosphorylated in response to EP_2 and EP_4 stimulation in the phosphoflow experiments. For EP_3 on the other hand, signaling through the $G_{\alpha i}$ pathway would be predicted to reduce PKA activity. No clear evidence for this was observed in the phosphoflow cytometry results. This could be due to lower expression of EP_3 and EP_1 than EP_2 and EP_4 in T cells (*26*), EP_3-mediated activation of additional intracellular signaling pathways through $G_{\alpha q}$, $G_{\alpha s}$, and $G_{\alpha 12}$ (*20*) that counterbalance $G_{\alpha i}$ signaling, or activation of certain adenylyl cyclase isoforms by $G_{\beta\gamma}$ signaling, increasing cAMP and activating PKA (*28*).The modeled networks for the EP_1 receptor recapitulated the $G_{\alpha q}$ signaling pathway with activation of PLC and PKC.

The literature suggests that $G_{\beta\gamma}$ signaling may be active downstream of EP_4 (*28*), EP_2 (*105*), and possibly also EP_3, when this receptor couples to $G_{\alpha i}$, the G_α protein most frequently associated with $G_{\beta\gamma}$ signaling (*75*, *106*). $G_{\beta\gamma}$ subunits can affect a number of different pathways including PI3K, PKA, PAK, Raf-1, and more (*75*), all of which we saw evidence for in either kinase prediction, motifs, or network models.

Evidence for G protein–independent PGE_2 signaling pathways from network modeling

There is some evidence in the literature that PGE_2 also triggers G protein–independent signaling. In particular, EP_2, EP_3, and EP_4 can couple to G protein–coupled receptor kinase (GRK) and β-arrestin (*28*, *107*, *108*), both of which can initiate their own signaling pathways (*76*, *77*, *109*). For instance, EPs may transactivate EGFR through β-arrestin and Src activation (*33*, *107*, *110–112*), which, in turn, triggers additional signaling pathways, including PI3K-Akt, Ras-Raf, and more (*19*). It is unclear whether this transactivation also occurs

in T cells, but in our inhibitor experiments, we observed that EGFR inhibition in T cells did affect some phosphoflow cytometry readouts. EGFR transactivation was also predicted in the modeled network for the combined stimulation condition in $CD8^+$ cells (fig. S22). By phosphoflow cytometry, EGFR and PI3K inhibitors affected many of the same pathways and readouts, for instance, CREB1 $pSer^{133}$, HSPB1 $pSer^{78}$, NDRG1 $pThr^{346}$, PKA substrates, and S6RP $pSer^{240}$ (Fig. 4E), possibly due to pathway convergence.

β-Arrestin can also trigger MAPKs (in particular, Raf and MAP3K5), PI3K, Ras homolog family member A (RhoA), and Src signaling pathways (*77*). Many of these were predicted in the modeled networks (Fig. 5, A to C). In support of RhoA signaling, several ARHGEFs, which are small GTPase activators, were regulated in the current dataset (Table 1 and table S3).

Other parts of the $EP_{1–4}$ inactivation process may also contribute to signaling output, and the data suggest some involvement of RGS proteins, for instance, through the regulation of phosphorylation of RGS3, RGS11, and RGS14 observed in the phosphoproteomics data. A few known GRK substrates were also regulated in the phosphoproteomics dataset, including sodium-hydrogen exchanger regulatory factor 1 (NHERF) and histone deacetylase (*109*), and GRKs were further predicted by NetPhorest to regulate some of the phosphosites seen by MS, mostly in CD8. Thus, the current study supports an important role for G protein–independent signaling alongside G protein–dependent signaling in PGE_2 signaling in T cells.

Concluding remarks

Here, we have conducted a system-level study of PGE_2 signaling pathways in helper, cytotoxic, and T_{reg} cell subsets. We present a comprehensive and detailed view of PGE_2-regulated signaling nodes, pathways, and networks in T cell subsets, thus improving the current understanding of PGE_2's multifaceted role in T cells and providing a valuable resource for targeted research on this physiologically and pathophysiologically important signaling system.

MATERIALS AND METHODS

Agonists and antagonists

EP_1 agonist ONO-DI-004, EP_2 agonist ONO-AE1-259-01, EP_3 agonist ONO-AE-248, EP_4 agonist ONO-AE1-329, EP_1 antagonist ONO-8713, and EP_3 antagonist ONO-AE3-240 were provided under a material transfer agreement with ONO Pharmaceuticals. EP_2 antagonist TG4-155 (catalog no. 17639) and EP_4 antagonist ONO-AE3-208 (catalog no. 14522) were both from Cayman Chemicals. PGE_2 (catalog no. P5640) was from Sigma-Aldrich.

Antibodies

CD3-peridinin-chlorophyll-protein (PerCP) clone SK7 (catalog no. 345766), CD4–phycoerythrin (PE)–Cy7 clone SK3 (catalog no. 348809), CD45RA allophycocyanin (APC)–H7 (catalog no. 560674), CD3-pacific blue (PB) clone UCHT1 (catalog no. 558117), CD4-PerCP (catalog no. 550631), CD8-PE-Cy7 (catalog no. 557746), forkhead box P3 (FOXP3)–Ax647 (catalog no. 560045), immunoglobulin G1 (IgG1) kappa-Ax647 (catalog no. 557783), CREB1 $pSer^{133}$/activating transcription factor 1 (ATF1) $pSer^{63}$-Ax647 (catalog no. 558434), histone H3 $pSer^{28}$-Ax647 (catalog no. 558217), S6RP $pSer^{240}$-Ax647 (catalog no. 560432), PKA RIIα (PRKAR2A) $pSer^{99}$-Ax647 (catalog no. 560164), and PKA RIIβ (PRKAR2B) $pSer^{114}$-Ax647 (catalog no. 560205) were from BD Biosciences. S6RP $pSer^{235/236}$-Ax647 (catalog no. 4851), histone H3 $pSer^{10}$-Ax647 (catalog no. 9716), NDRG1 $pThr^{346}$-Ax647 (catalog no. 7497), pPKA substrate (RRXS/T) (catalog no. 9624), PLCγ-1 (PLCG1) $pThr^{783}$ (catalog no. 2821), p-Akt substrate (RXRXXS/T) (catalog no. 9614), GSK3α (GSK3A) $pSer^{21}$ (catalog no. 9316), HSP27 (HSPB1) $pSer^{78}$ (catalog no. 2405), VASP $pSer^{157}$ (catalog no. 3111), and PKA-C (PRKACA) $pThr^{197}$ (catalog no. 4781) were from Cell Signaling Technology (CST). CD25-PE clone 4E3 (catalog no. 130-091-024) was from Miltenyi Biotec. CD127-PECy7 clone RDR5 (catalog no. 25-1278-73) was from eBioscience. Pacific Blue succinimidyl ester (catalog no. P10163), Alexa Fluor 488 succinimidyl ester (catalog no. A3005), Pacific Orange succinimidyl ester (catalog no. P30253), Goat anti-mouse IgG1 secondary antibody Ax647 (catalog no. A21240), and Goat anti-rabbit IgG secondary antibody Ax647 (catalog no. A21245) were from Thermo Fisher Scientific. VIM $pSer^{38}$ (catalog no. Ab52942) was from Abcam.

Kinase inhibitors

PKA inhibitor H89 (catalog no. 10010556, Cayman Chemicals), PI3K inhibitor Wortmannin (catalog no. W1628, Sigma-Aldrich), PI3K inhibitor LY294002 (catalog no. 9901, CST), MEK inhibitor CI-1040 (catalog no. Sc-202759, Santa Cruz Biotechnology), Src inhibitor PP2 (catalog no. 529573, Calbiochem), GSK3 inhibitor CT99021 (catalog no. Axon 1386, Axon Medchem), CK2 inhibitor TBB (catalog no. 2275, Tocris), and EGFR inhibitor AG1478 (catalog no. S2728, Selleck Chemicals).

Patient material and ethical considerations

Buffy coats were obtained from anonymized healthy blood donors [Oslo University Hospital Blood Centre, Oslo, Norway; studies were approved by the Regional Ethics Committee, all donors gave their consent, and the research on human blood was carried out in accordance with the Declaration of Helsinki (2013)].

Purification of CD3, CD4, CD8, and T_{reg} cells

Human peripheral blood CD3, CD4, and CD8 T cells were isolated from buffy coats from healthy blood donors using RosetteSep Enrichment Kits for CD3, CD4, or CD8 cells (STEMCELL Technologies) followed by gradient centrifugation with LymphoPrep (Axis Shield) according to the manufacturer's protocol but using phosphate-buffered saline (PBS) instead of 2% fetal calf serum (FCS) (Thermo Fisher Scientific) in PBS during washes. For T_{reg} isolation, CD4 cells isolated as described above were processed using the $CD4^+CD25^+CD127^{dim/–}$ Regulatory T Cell Isolation Kit II (Miltenyi Biotec) according to the manufacturer's protocol. Cells were then suspended to 1×10^6 cells/ml in X-VIVO 15 medium (Lonza) with 10% FCS (Invitrogen), 1× penicillin-streptomycin (Thermo Fisher Scientific), 100 nM rapamycin (Calbiochem), and recombinant IL-2 (500 U/ml; Invitrogen). A total of 100,000 cells were plated per well in 96-well plates, and 400,000 CD3/CD28 MACSibeads (T cell Activation/Expansion Kit, Miltenyi Biotech, prepared according to the manufacturer's instructions) were added. Medium was replaced on day 1 after plating and then every 4 to 5 days until cells were harvested at day 14 after plating. Cells were moved to larger well plates at appropriate times during expansion.

Stimulation of cells for MS

For stimulation, cells were suspended in RPMI 1640 GlutaMax medium (Thermo Fisher Scientific) and diluted to 20×10^6 cells/ml. Aliquots (1 ml) were then equilibrated in a 37°C water bath for 30 min before stimulation. CD4, CD8, or T_{reg} cells (20 million per condition) were stimulated with 1 μM EP_1 agonist (ONO-DI-004),

0.04 μM EP_2 agonist (ONO-AE1-259-01), 0.05 μM EP_3 agonist (ONO-AE-248), 0.052 μM EP_4 agonist (ONO-AE1-329) [all at 10× median effective concentration (EC_{50}) except ONO-DI-004, which was used at 2.5× EC_{50}], 10 μM PGE_2, or vehicle for 5 min. Stimulation concentrations used were based on titration experiments by flow cytometry as well as recommendations provided by ONO Pharmaceuticals. Cells were then centrifuged (400*g*, 2 min, 4°C), the supernatant was removed, and the pellet was snap-frozen on liquid nitrogen. For each cell type, buffy coats from five healthy blood donors were used, providing five biological replicates.

Protein lysis and digestion

Cells were lysed at 4°C with a Bioruptor Plus (Diagenode) for 15 cycles of 30 s, in buffer containing 50 mM ammonium bicarbonate (pH 8.0), 8 M urea, 1 mM sodium orthovanadate, cOmplete EDTA-free protease inhibitor mixture, and phosSTOP phosphatase inhibitor mixture (both Roche). Cell debris was then removed by centrifugation at 20,000*g* for 10 min at 4°C. The total protein concentration was measured using a Bradford assay (Bio-Rad). Proteins were reduced with dithiothreitol at a final concentration of 4 mM at 56°C for 25 min; subsequently, samples were alkylated with iodoacetamide at a final concentration of 8 mM at room temperature for 30 min in the dark. Proteins were then predigested using Lys-C (enzyme:substrate ratio of 1:100) for 4 hours at 37°C. The solution was then diluted to a final urea concentration of 2 M with 50 mM ammonium bicarbonate (pH 8.0), prior trypsin digestion at 37°C overnight (enzyme:substrate ratio of 1:100). The digestion was quenched by acidification to 5% of formic acid. The digests were desalted using Sep-Pak C18 cartridges (Waters), dried in vacuo, and stored at −80°C until further use.

Phosphopeptide enrichment by Ti^{4+}-IMAC

Ti^{4+}-IMAC material was prepared and used essentially as previously described (*113*). In-parallel spin tip enrichment (*55*) by centrifugation at 50 to 100*g* was performed as follows: Columns were conditioned using 50 μl of loading buffer [80% acetonitrile/6% trifluoroacetic acid (TFA)], 200 μg of protein digests dissolved in loading buffer were loaded, and then the columns were sequentially washed with 50 μl of 50% acetonitrile (ACN), 0.5% TFA containing 200 mm NaCl, and 50 μl of 50% ACN/0.1% TFA. The bound phosphopeptides were eluted into a new tube (containing 30 μl of 10% formic acid) with 20 μl of 10% ammonia. A final elution was performed with 10 μl of 80% ACN/2% formic acid. The collected eluate was further acidified by the addition of 5 μl of 100% formic acid, dried in vacuo, and desalted using C18-StageTips (*114*), before nanoscale liquid chromatography–tandem MS (nLC-MS/MS) analysis.

Reverse phase chromatography and MS

Peptides were subjected to reverse-phase nLC-MS/MS analysis using a Proxeon EASY-nLC 1000 (Thermo Fisher Scientific) and an LTQ (Linear Trap Quadropole)–Orbitrap Elite (Thermo Fisher Scientific) or using the Agilent 1290 Infinity UHPLC (Ultra High Performance Liquid Chromatography) System (Agilent) and an Orbitrap Fusion mass spectrometer (Thermo Fisher Scientific). Peptides were first trapped (Reprosil C18, Dr. Maisch; 3 μm, 2 cm by 100 μm) at 5 μl/min with 100% solvent A (0.1% formic acid in water) before being separated on the analytical column (Agilent Poroshell 120 EC-C18, Agilent; 2.7 μm, 40 cm by 50 μm). Peptides were chromatographically separated by a 90-min gradient from 7 to 30% (or 95-min gradient from 4 to 36% for the Agilent 1290) of solvent B (0.1% formic acid in 80% ACN) at a flow rate of ~100 nl/min. The total measurement time for each sample was 110 min. The mass spectrometer was operated in a data-dependent mode to automatically switch between MS and MS/MS. Briefly, survey full-scan MS spectra were acquired in the Orbitrap analyzer, scanning from mass/charge ratio (m/z) 350 to m/z 1500 at a resolution of 60,000 using an automatic gain control setting of 1×10^6 ions (or 4×10^5 for the Orbitrap Fusion). Charge state screening was enabled, and precursors with either unknown or 1+ charge states were excluded. After the MS survey scan, the 20 most intense precursors were selected for subsequent collision-induced dissociation (CID) or ETD fragmentation by a decision tree–based method (*115*) with ion trap readout. The normalized collision energy for CID was set at 35%, and supplemental activation for ETD and dynamic exclusion were enabled (40 or 18 s for the Agilent 1290).

Data analysis

Raw files were processed using MaxQuant (version 1.5.2.8) (*116*). Proteins and peptides were identified using a target-decoy approach with a reversed database, using the Andromeda search engine integrated into the MaxQuant environment. The database search was performed against the human Swiss-Prot database (version August, 2014) and against a common contaminant database. Default settings were used, with the following minor changes: oxidation (M), acetyl (protein N-term), and phospho (STY) as variable modifications. Enzyme specificity was set to trypsin with a maximum of two missed cleavages and a minimum peptide length of six amino acids. A false discovery rate (FDR) of 1% was applied at the protein, peptide, and modification level. A site localization probability of at least 0.75 was used as thresholds for the localization of phosphorylated residues. The "match between runs" feature was enabled.

Bioinformatics analysis was performed with Perseus (*117*) and R statistical computing software (*118*). The three datasets were processed individually, and data were filtered to make sure that identified phosphorylation sites showed quantification value in all five biological replicates of at least one stimulation, and missing values were then imputed on the basis of normal distribution (down shift = 1.8, width = 0.15), as implemented in the Perseus software (*117*). Significance was assessed by *t* test with a permutation-based FDR of 5% and a S0 parameter (within groups variance) of 0.1.

Venn diagrams were produced using the following tool: http://bioinformatics.psb.ugent.be/webtools/Venn/. Significantly regulated phosphorylation sites were subjected to IceLogo (*119*), using percent difference compared to the reference set Swiss-Prot means for *Homo Sapiens*, with a significance set to 0.05. Kinases responsible for regulating the observed regulated phosphosites were predicted using the tool NetPhorest (*58*). The sequence database used was "Human – Uniprot 2013/01 (MaxQuant)." Default settings were used, with minimum score = 2 and max difference = 4. The max number of predictions was set to 1. The tool PFP (www.kiharalab.org/web/pfp.php) (*61*) was used to predict which of the regulated phosphosites observed in the current study are likely to be functional. The database was downloaded on 30 March 2013, version "pfp_database_release_1_2_update_1__20160126.csv.zip." Regulated phosphosites were searched against the database, and lists compiled of regulated phosphosites that were actual class positive (known-function human phosphosites from the PhosphoSitePlus database, file name: Regulatory_sites, version: 060415) and regulated phosphosites that were either actual class positive or that have at least one positive prediction (in RandomForest, BayesNet, Logistic, or Multilayer Perceptron

models). GO analysis was performed using the ClueGO cytoscape plugin (*120*). Regulated proteins in each condition were searched against the Kyoto Encyclopedia of Genes and Genomes (KEGG), GO Biological Process–EBI-QuickGO-GOA, and Wikipathways databases using the following ClueGO parameters: GO term fusion selected, show only pathways with $P \leq 0.05$, GO Tree Interval = all levels, GO term minimum number of genes = 3, 4% of genes per pathway, and kappa score = 0.42. Regulated immune processes were identified by querying the regulated proteins against the GO ImmuneSystemProcess-EBI-QuickGO-GOA database. The MS proteomics data have been deposited in the ProteomeXchange Consortium through the Proteomics Identification Database (PRIDE) partner repository (*121*) with the dataset identifier PXD014503.

Isolation, stimulation, and fixation of cells for phosphoflow cytometry

CD3 cells were resuspended in RPMI 1640 GlutaMAX medium (Thermo Fisher Scientific) and preequilibrated for 10 min in a 37°C water bath before preincubation with kinase inhibitors, antagonists, or stimulation with EP_{1-4} agonists, PGE_2, or dimethyl sulfoxide (DMSO) control (maximum total DMSO concentration of 0.3%). Antagonists were added 5 min before stimulation, and inhibitors were added 30 min before stimulation. Agonists and antagonists were used at the following concentrations, except where indicated otherwise: EP_1 agonist ONO-DI-004 (1 μM), EP_2 agonist ONO-AE1-259-01 (40 nM), EP_3 agonist ONO-AE-248 (50 nM), EP_4 agonist ONO-AE1-329 (52 nM), EP_1 antagonist ONO-8713 (1 μM), EP_2 antagonist TG4-155 (150 nM), EP_3 antagonist ONO-AE3-240 (150 nM), and EP_4 antagonist ONO-AE3-208 (100 nM). Inhibitors were used at the following concentrations: PKA inhibitor H89 (20 μM), PI3K inhibitor Wortmannin (1 μM), PI3K inhibitor LY294002 (10 μM), MEK inhibitor CI-1040 (2 μM), Src inhibitor PP2 (10 μM), GSK3 inhibitor CT99021 (2 μM), CK2 inhibitor TBB (10 μM), and EGFR inhibitor AG1478 (10 μM).

At the indicated time points, samples were harvested by fixation for 10 min with prewarmed Phosphoflow Fix Buffer I (catalog no. 557870, BD Biosciences) at 37°C followed by two washes with PBS. An unstimulated sample was collected before stimulation.

Fluorescent cell barcoding

Fixed cells were incubated with different concentrations of NHS-coupled Alexa Fluor 488, Pacific Orange, and Pacific Blue in a 96-well V-bottom plate for 20 min in the dark at room temperature. Cells were washed twice with flow buffer (PBS and 2% FCS), combined, permeabilized with ice-cold Phosphoflow Perm Buffer III (BD Biosciences, catalog no. 558050), and then stored at −80°C until analysis.

Antibody staining and phosphoflow cytometry

Permeabilized cells were thawed on ice and washed once with flow buffer. Cells were then resuspended in flow buffer and plated in a 96-well V-bottom plate. Cells were stained with PerCP-conjugated anti-CD3, PE-Cy7–conjugated anti-CD4, APC-H7–conjugated anti-CD45RA, and the indicated phosphoantibodies at room temperature, in the dark for 30 min. Cells were then washed twice with flow buffer. For unconjugated phosphoantibodies, a second staining step was performed with Ax647-conjugated secondary antibody for 30 min in the dark, followed by two washes with flow buffer. Cells were then analyzed on an LSR Fortessa flow cytometer (BD Biosciences). Compensation was performed using unstimulated cells stained with Alexa Fluor 488, Pacific Orange, and Pacific Blue, as well as compensation beads incubated with PerCP-, PE-Cy7–, APC-H7–, and Ax647-conjugated antibodies. One hundred fifty thousand to 1 million events were recorded per sample.

Phosphoflow cytometry data analysis

The data were analyzed in Cytobank (https://cellmass.cytobank.org/cytobank/). Lymphocytes were selected by plotting side scatter area (SSC-A) versus forward scatter-area (FSC-A). Singlets were selected by plotting FSC-height (H) versus FSH-width (W). Each barcoding channel was then plotted against SSC-A to identify the different barcoding populations. Subsequently, cells were gated for CD3, CD4, and CD45RA. CD4 and CD8 cells were identified by the presence or absence of the CD4 marker, whereas CD45RA and CD45RO cells were identified by the presence or absence of the CD45RA marker. Signals for the phosphoantibodies were calculated as inverse hyperbolic sine (arcsinh) ratios of mean fluorescence intensities (MFIs) for stimulated versus unstimulated cells. Statistical analyses were performed in GraphPad Prism 7.02 (GraphPad Software). For median inhibitory concentration (IC_{50}) and EC_{50} calculations, a three-parameter nonlinear regression was used, with the Hill coefficient set to 1. The equations used were $Y = \text{Bottom} + (\text{Top} - \text{Bottom})/(1 + 10^{(\log EC50 - X)})$ and $Y = \text{Bottom} + (\text{Top} - \text{Bottom})/(1 + 10^{(X - \log IC50)})$.

Network modeling with PHONEMeS

PHONEMeS requires the use of a Prior Knowledge Network (PKN). First, the PKN is formalized as a Boolean model. Then, the Boolean model is trained with experimental data to find which interactions are relevant in the context of the present study. For assembling our PKN, we used OmniPath (*122*), a comprehensive collection of 57 pathway resources (http://omnipathdb.org/info). As a first step, we built the PKN by including all the K/P-S interactions from OmniPath. Because there were no connecting paths between GPCRs and measured phosphosites in the K/P-S network alone, we mapped proteins involved in GPCR downstream signaling (obtained from MSigDb, http://software.broadinstitute.org/gsea/msigdb/cards/REACTOME_GPCR_DOWNSTREAM_SIGNALING) (*123*), on the signed and directed protein-protein interactions of OmniPath to create a GPCR downstream signaling causal network. This network was then combined with the K/P-S network and a list of manually curated interactions from the literature (data file S2). In addition, functionally related G protein subunits and other proteins in the PKN were grouped together (data file S3). This yielded a list of 26,367 interactions, 2414 of which are signed and directed protein interactions, whereas the rest is all the set of K/P-S interactions now present in OmniPath. We use this PKN to train and contextualize the cell type–specific signalling networks for CD4 and CD8. The next step consists of preparing the data inputs for PHONEMeS. Sites that have no interaction evidence in the PKN will be ignored. Significantly regulated sites for each cell type were identified through statistical testing with a permutation-based FDR (Benjamini-Hochberg method) at a threshold value of $p\text{Thresh} = 0.05$ for CD4 and CD8 cell types. We assigned to each of the measurements i at each experimental condition j (EP_1, EP_2, EP_3, EP_4, and PGE_2) a score based on their inferred adjusted P values $S_{i,j} = \log_2(p\text{Val}_{i,j}/p\text{Thresh})$. Significantly regulated sites (with $p\text{Val}_{i,j} < 0.05$) are assigned a negative score ($S_{i,j} < 0$), whereas the rest of measurements (with $p\text{Val}_{i,j} \geq 0.05$) are assigned a positive score ($S_{i,j} > 0$). An ILP implementation of PHONEMeS

was used for training the network to the input data. The ILP formulation consists of two main parts: an objective function and a set of linear constraints whose variables are all binaries (indicating the presence/absence of a node or interaction in the optimal solution). The objective function represents the cost function of the ILP problem. In this case, it is defined as a minimization of the sum of scores assigned to each node (each node representing a specific site) on each of the conditions considered for the PHONEMeS analysis. Because this is a minimization problem, the method incorporates as many regulated sites (with negative score assigned $S_{i,j} < 0$) while penalizing the inclusion of the nonregulated measurements (which were assigned a positive score $S_{i,j} > 0$). In addition, a set of constraints in the ILP formulation determines the set of feasible paths connecting the upstream prostaglandin receptors with the downstream measurements. In this case, a feasible path is a set of interactions present in the PKN connecting the prostaglandin receptors with the measurements through intermediate nodes. A size penalty factor ($\lambda = 0.0001$) over the number of interactions is also applied in the objective function, so as to systematically apply Occam's razor to the final set of networks. This size penalty is small compared to the scores (in absolute values) assigned to each measured node and is added such that simpler models (with fewer edges in the solution) are preferred over the larger ones. The ILP problem is solved through the CPLEX-IBM optimizer.

Codes for the modeling are available at https://github.com/saezlab/Prostaglandin_Project.

Phenotyping of CD4, CD8, and T_{regs} for MS

To verify the purity of the isolated CD4 and CD8 cells used for MS studies, cell samples were fixed and permeabilized using Phosflow buffers (BD Biosciences), followed by staining (20 min at room temperature) for relevant surface markers. For CD4 cells, CD3-PerCP (1 or 100 μl of final volume) and CD4–PE-Cy7 (1 or 100 μl of final volume) were used. For CD8 cells, CD3-PB (0.5 or 100 μl of final volume), CD4-PerCP (2 or 100 μl of final volume), and CD8–PE-Cy7 (0.2 or 100 μl of final volume) were used. All antibodies were from BD Biosciences.

To confirm the purity of the expanded T_{regs}, a small sample of the cells used for MS studies were fixed, permeabilized with FOXP3 buffers (BD Biosciences) according to the manufacturer's instructions, and then stained for 20 min at room temperature with the following antibodies against cell surface markers: CD3–Pacific Blue (0.5 or 100 μl of final volume; BD Biosciences), CD4-PerCP (2 or 100 μl of final volume; BD Biosciences), CD25-PE (5 or 100 μl of final volume; Miltenyi Biotec), FOXP3-Ax647 (5 or 100 μl of final volume, BD Biosciences), and CD127-PECy7 (0.25 or 100 μl of final volume; eBioscience).

T_{reg} suppression assay

T_{eff} responder cells ($CD4^+CD25^-$) were isolated from buffy coats from healthy human donors by first purifying CD4 cells as described in the "Purification of CD3, CD4, CD8, and T_{reg} cells" section and then depleting CD25 cells within this population. To deplete CD25 cells, CD4 cells were first suspended in MACSi buffer (PBS with 0.5% bovine serum albumin and 2 mM EDTA) at 10^7 cells per 80 μl of buffer. Anti-CD25 microbeads (20 μl; Miltenyi Biotec) were added per 10^7 cells and incubated on ice for 15 min, followed by addition of 50 ml of MACSi buffer and centrifugation (350*g*, 10 min). Supernatant was removed, and cells were suspended in 1.5 ml of MACSi buffer. An LD column (Miltenyi Biotec) was placed in magnetic holder, wetted with 2 ml of MACSi buffer, and followed by loading of cells. Cells were allowed to pass through by gravity, followed by rinsing of the column twice with 1 ml of MACSi buffer. Eluate was washed twice with RPMI, followed by labeling with 2 μM carboxyfluorescein diacetate succinimidyl ester (CFSE; Sigma-Aldrich) in RPMI for 10 min at 37°C. Volume (10×) of 100% cold FCS was added to quench the labeling reaction, followed by washing with 10% FCS in RPMI.

To test suppression of T_{eff} proliferation by T_{regs}, 200,000 CFSE-labeled T_{eff} cells were plated in 10% FCS in RPMI in round-bottom 96-well plates together with varying numbers of T_{regs}. Cells were stimulated with 42,000 CD2/CD3/CD28 MACSibeads (T cell Activation/Expansion Kit, Miltenyi Biotech, prepared according to the manufacturer's instructions). Cells were allowed to proliferate for 4 days in a 37°C incubator, then fixed with FOXP3 buffer A (BD Biosciences), frozen, and then run on an LSR Fortessa.

FOXP3 promoter methylation

To assess methylation levels of the FOXP3 promoter, which is an indicator of bona fide T_{reg} status, DNA was isolated using the DNeasy kit (Qiagen) from expanded T_{regs}. Cells from two healthy buffy coats were used, and T_{regs} were isolated and expanded as described in the "Purification of CD3, CD4, CD8, and T_{reg} cells" section. After DNA extraction, unmethylated cytosines were converted to uracils using sodium bisulfite conversion (Epitect Bisulfite Kit from Qiagen). Converted DNA was subjected to polymerase chain reaction (PCR) amplification with primers Fxpro-met_F1 and Fxpro-met_R2 (*124*), Taq polymerase (Invitrogen), and the following thermocycler conditions: 15 min at 94°C, 40 cycles in 1 min at 94°C, 45 s at 60°C, 1 min at 72°C, and then a final extension period of 10 min at 72°C. PCR products were cleaned up using a PCR purification kit (Saveen) and cloned into a sequencing vector using the pGEM-T Easy Vector Systems (Promega) according to the manufacturer's protocol. At least 10 clones were sequenced for each donor/cell type, and the demethylation of 10 CpG methylation sites within the T_{reg}-specific demethylated region was assessed (−256, −216, −139, −127, −114, −78, −66, −59, −44, and −16).

Western blots

CD4, CD8, and T_{reg} cells were isolated/expanded as described in the "Purification of CD3, CD4, CD8, and T_{reg} cells" section. Frozen pellets were lysed in 200 μl of radioimmunoprecipitation assay with cOmplete protease inhibitor tablets (Roche) for 10 min on ice. Samples were then sonicated 10× and centrifuged (16.1*g*, 10 min, 4°C), and the protein concentration of the supernatant was determined by Bradford assay. Protein (65 μg) was loaded per lane on precast SDS–polyacrylamide gel electrophoresis gels (Bio-Rad), which were run at 120 V for 1 hour and 45 min. Transfer onto an Immobilon-P polyvinylidene difluoride membrane (Merck) proceeded at room temperature for 1 hour at 100 V. Membranes were blocked in 5% milk in Tris-buffered saline with 0.1% Tween-20 (TBS-T) in cold room overnight. Staining with primary antibodies diluted in 5% milk in TBS-T EP_1 receptor polyclonal antibody at 1:200 (item no. 101740, Cayman Chemicals), EP_2 receptor polyclonal antibody at 1:1000 (item no. 101750, Cayman Chemicals), PTGER3/EP_3 antibody at 1:2000 (item NBP1-00810, Novus Biologicals), PTGER4/EP_4 antibody at 1:1000 (item NBP1-84833, Novus Biologicals), or actin C-11 at 1:2000 (Santa Cruz Biotechnology) proceeded

for 90 min at room temperature, followed by washing three times with TBS-T. Membranes were then incubated with Peroxidase-AffiniPure Goat Anti-Rabbit IgG (H+L) secondary antibody (Jackson ImmunoResearch) for 90 min at 1:10,000 dilution in 5% milk in TBS-T, followed by three washes with TBS-T. Membranes were then developed with SuperSignal West Dura Extended Duration Substrate (Pierce).

SUPPLEMENTARY MATERIALS

www.science.org/doi/10.1126/scisignal.abc8579
Figs. S1 to S22
Tables S1 to S5
Data files S1 to S3
Reference (*124*)

View/request a protocol for this paper from *Bio-protocol*.

REFERENCES AND NOTES

1. K. W. Brudvik, K. Tasken, Modulation of T cell immune functions by the prostaglandin E(2) - cAMP pathway in chronic inflammatory states. *Br. J. Pharmacol.* **166**, 411–419 (2012).
2. V. Sreeramkumar, M. Fresno, N. Cuesta, Prostaglandin E2 and T cells: Friends or foes? *Immunol. Cell Biol.* **90**, 579–586 (2012).
3. M. T. Wang, K. V. Honn, D. Nie, Cyclooxygenases, prostanoids, and tumor progression. *Cancer Metastasis Rev.* **26**, 525–534 (2007).
4. M. Mahic, S. Yaqub, C. C. Johansson, K. Taskén, E. M. Aandahl, FOXP3$^+$CD4$^+$CD25$^+$ adaptive regulatory T cells express cyclooxygenase-2 and suppress effector T cells by a prostaglandin E2-dependent mechanism. *J. Immunol.* **177**, 246–254 (2006).
5. A. Greenhough, H. J. M. Smartt, A. E. Moore, H. R. Roberts, A. C. Williams, C. Paraskeva, A. Kaidi, The COX-2/PGE2 pathway: Key roles in the hallmarks of cancer and adaptation to the tumour microenvironment. *Carcinogenesis* **30**, 377–386 (2009).
6. N. Obermajer, P. Kalinski, Generation of myeloid-derived suppressor cells using prostaglandin E2. *Transplant Res.* **1**, 15 (2012).
7. L. Martinet, C. Jean, G. Dietrich, J. J. Fournié, R. Poupot, PGE2 inhibits natural killer and gamma delta T cell cytotoxicity triggered by NKR and TCR through a cAMP-mediated PKA type I-dependent signaling. *Biochem. Pharmacol.* **80**, 838–845 (2010).
8. D. M. Holt, X. Ma, N. Kundu, P. D. Collin, A. M. Fulton, Modulation of host natural killer cell functions in breast cancer via prostaglandin E2 receptors EP2 and EP4. *J. Immunother.* **35**, 179–188 (2012).
9. D. Wang, R. N. DuBois, An inflammatory mediator, prostaglandin E2, in colorectal cancer. *Cancer J.* **19**, 502–510 (2013).
10. D. Wang, R. N. DuBois, The role of prostaglandin E_2 in tumor-associated immunosuppression. *Trends Mol. Med.* **22**, 1–3 (2016).
11. P. Sinha, V. K. Clements, A. M. Fulton, S. Ostrand-Rosenberg, Prostaglandin E2 promotes tumor progression by inducing myeloid-derived suppressor cells. *Cancer Res.* **67**, 4507–4513 (2007).
12. F. Baratelli, Y. Lin, L. Zhu, S. C. Yang, N. Heuzé-Vourc'h, G. Zeng, K. Reckamp, M. Dohadwala, S. Sharma, S. M. Dubinett, Prostaglandin E2 induces FOXP3 gene expression and T regulatory cell function in human CD4$^+$ T cells. *J. Immunol.* **175**, 1483–1490 (2005).
13. S. Sharma, S. C. Yang, L. Zhu, K. Reckamp, B. Gardner, F. Baratelli, M. Huang, R. K. Batra, S. M. Dubinett, Tumor cyclooxygenase-2/prostaglandin E2-dependent promotion of FOXP3 expression and CD4+ CD25+ T regulatory cell activities in lung cancer. *Cancer Res.* **65**, 5211–5220 (2005).
14. P. M. Rothwell, M. Wilson, C. E. Elwin, B. Norrving, A. Algra, C. P. Warlow, T. W. Meade, Long-term effect of aspirin on colorectal cancer incidence and mortality: 20-year follow-up of five randomised trials. *Lancet* **376**, 1741–1750 (2010).
15. P. M. Rothwell, M. Wilson, J. F. Price, J. F. F. Belch, T. W. Meade, Z. Mehta, Effect of daily aspirin on risk of cancer metastasis: A study of incident cancers during randomised controlled trials. *Lancet* **379**, 1591–1601 (2012).
16. J. Cuzick, M. A. Thorat, C. Bosetti, P. H. Brown, J. Burn, N. R. Cook, L. G. Ford, E. J. Jacobs, J. A. Jankowski, C. la Vecchia, M. Law, F. Meyskens, P. M. Rothwell, H. J. Senn, A. Umar, Estimates of benefits and harms of prophylactic use of aspirin in the general population. *Ann. Oncol.* **26**, 47–57 (2015).
17. S. J. Bains, M. Mahic, T. Å. Myklebust, M. C. Småstuen, S. Yaqub, L. M. Dørum, B. A. Bjørnbeth, B. Møller, K. W. Brudvik, K. Taskén, Aspirin as secondary prevention in patients with colorectal cancer: An unselected population-based study. *J. Clin. Oncol.* **34**, 2501–2508 (2016).
18. A. T. Chan, S. Ogino, C. S. Fuchs, Aspirin use and survival after diagnosis of colorectal cancer. *JAMA* **302**, 649–658 (2009).
19. G. O'Callaghan, A. Houston, Prostaglandin E2 and the EP receptors in malignancy: Possible therapeutic targets? *Br. J. Pharmacol.* **172**, 5239–5250 (2015).
20. D. F. Woodward, R. L. Jones, S. Narumiya, International Union of Basic and Clinical Pharmacology. LXXXIII: Classification of prostanoid receptors, updating 15 years of progress. *Pharmacol. Rev.* **63**, 471–538 (2011).
21. S. Zelenay, A. G. van der Veen, J. P. Böttcher, K. J. Snelgrove, N. Rogers, S. E. Acton, P. Chakravarty, M. R. Girotti, R. Marais, S. A. Quezada, E. Sahai, C. Reis e Sousa, Cyclooxygenase-dependent tumor growth through evasion of immunity. *Cell* **162**, 1257–1270 (2015).
22. K. Newick, S. O'Brien, J. Sun, V. Kapoor, S. Maceyko, A. Lo, E. Puré, E. Moon, S. M. Albelda, Augmentation of CAR T-cell trafficking and antitumor efficacy by blocking protein kinase a localization. *Cancer Immunol. Res.* **4**, 541–551 (2016).
23. "Study of ONO-4578 With and Without ONO-4538 in Subjects Advanced or Metastatic Solid Tumors," draft, 10 April 2017; https://ClinicalTrials.gov/show/NCT03155061.
24. Y. Sugimoto, S. Narumiya, Prostaglandin E receptors. *J. Biol. Chem.* **282**, 11613–11617 (2007).
25. S. L. Tilley, T. M. Coffman, B. H. Koller, Mixed messages: Modulation of inflammation and immune responses by prostaglandins and thromboxanes. *J. Clin. Invest.* **108**, 15–23 (2001).
26. K. Boniface, K. S. Bak-Jensen, Y. Li, W. M. Blumenschein, M. J. McGeachy, T. K. McClanahan, B. S. McKenzie, R. A. Kastelein, D. J. Cua, R. de Waal Malefyt, Prostaglandin E2 regulates Th17 cell differentiation and function through cyclic AMP and EP2/EP4 receptor signaling. *J. Exp. Med.* **206**, 535–548 (2009).
27. C. Nataraj, D. W. Thomas, S. L. Tilley, M. T. Nguyen, R. Mannon, B. H. Koller, T. M. Coffman, Receptors for prostaglandin E_2 that regulate cellular immune responses in the mouse. *J. Clin. Invest.* **108**, 1229–1235 (2001).
28. U. Yokoyama, K. Iwatsubo, M. Umemura, T. Fujita, Y. Ishikawa, The prostanoid EP4 receptor and its signaling pathway. *Pharmacol. Rev.* **65**, 1010–1052 (2013).
29. H. Fujino, K. A. West, J. W. Regan, Phosphorylation of glycogen synthase kinase-3 and stimulation of T-cell factor signaling following activation of EP2 and EP4 prostanoid receptors by prostaglandin E2. *J. Biol. Chem.* **277**, 2614–2619 (2002).
30. H. Fujino, J. W. Regan, EP(4) prostanoid receptor coupling to a pertussis toxin-sensitive inhibitory G protein. *Mol. Pharmacol.* **69**, 5–10 (2006).
31. K. S. Chun, H. C. Lao, C. S. Trempus, M. Okada, R. Langenbach, The prostaglandin receptor EP2 activates multiple signaling pathways and beta-arrestin1 complex formation during mouse skin papilloma development. *Carcinogenesis* **30**, 1620–1627 (2009).
32. J. I. Kim, V. Lakshmikanthan, N. Frilot, Y. Daaka, Prostaglandin E_2 promotes lung cancer cell migration via EP4-βArrestin1-c-Src signalsome. *Mol. Cancer Res.* **8**, 569–577 (2010).
33. S. Tan, X. Chen, M. Xu, X. Huang, H. Liu, J. Jiang, Y. Lu, X. Peng, B. Wu, PGE_2/EP_4 receptor attenuated mucosal injury via β-arrestin1/Src/EGFR-mediated proliferation in portal hypertensive gastropathy. *Br. J. Pharmacol.* **174**, 848–866 (2017).
34. F. G. Buchanan, D. L. Gorden, P. Matta, Q. Shi, L. M. Matrisian, R. N. DuBois, Role of beta-arrestin 1 in the metastatic progression of colorectal cancer. *Proc. Natl. Acad. Sci. U.S.A.* **103**, 1492–1497 (2006).
35. S. M. DeWire, S. Ahn, R. J. Lefkowitz, S. K. Shenoy, β-Arrestins and cell signaling. *Annu. Rev. Physiol.* **69**, 483–510 (2007).
36. L. M. Luttrell, W. E. Miller, Arrestins as regulators of kinases and phosphatases. *Prog. Mol. Biol. Tramsl. Sci.* **118**, 115–147 (2013).
37. A. M. Lone, K. Taskén, Proinflammatory and immunoregulatory roles of eicosanoids in T cells. *Front. Immunol.* **4**, 130 (2013).
38. M. Nakanishi, A. Menoret, T. Tanaka, S. Miyamoto, D. C. Montrose, A. T. Vella, D. W. Rosenberg, Selective PGE(2) suppression inhibits colon carcinogenesis and modifies local mucosal immunity. *Cancer Prev. Res. (Phila.)* **4**, 1198–1208 (2011).
39. M. Zeddou, R. Greimers, N. de Valensart, B. Nayjib, K. Tasken, J. Boniver, M. Moutschen, S. Rahmouni, Prostaglandin E2 induces the expression of functional inhibitory CD94/NKG2A receptors in human CD8+ T lymphocytes by a cAMP-dependent protein kinase A type I pathway. *Biochem. Pharmacol.* **70**, 714–724 (2005).
40. V. Ganapathy, T. Gurlo, H. O. Jarstadmarken, H. von Grafenstein, Regulation of TCR-induced IFN-gamma release from islet-reactive non-obese diabetic CD8$^+$ T cells by prostaglandin E_2 receptor signaling. *Int. Immunol.* **12**, 851–860 (2000).
41. F. G. Snijdewint, P. Kalinski, W. A. Wierenga, J. D. Bos, M. L. Kapsenberg, Prostaglandin E2 differentially modulates cytokine secretion profiles of human T helper lymphocytes. *J. Immunol.* **150**, 5321–5329 (1993).
42. T. Vang, K. M. Torgersen, V. Sundvold, M. Saxena, F. O. Levy, B. S. Skålhegg, V. Hansson, T. Mustelin, K. Taskén, Activation of the COOH-terminal Src kinase (Csk) by cAMP-dependent protein kinase inhibits signaling through the T cell receptor. *J. Exp. Med.* **193**, 497–508 (2001).
43. A. Ruppelt, R. Mosenden, M. Grönholm, E. M. Aandahl, D. Tobin, C. R. Carlson, H. Abrahamsen, F. W. Herberg, O. Carpén, K. Taskén, Inhibition of T cell activation by cyclic adenosine 5′-monophosphate requires lipid raft targeting of protein kinase A type I by the A-kinase anchoring protein ezrin. *J. Immunol.* **179**, 5159–5168 (2007).
44. R. Mosenden, P. Singh, I. Cornez, M. Heglind, A. Ruppelt, M. Moutschen, S. Enerbäck, S. Rahmouni, K. Taskén, Mice with disrupted type I protein kinase A anchoring in T cells resist retrovirus-induced immunodeficiency. *J. Immunol.* **186**, 5119–5130 (2011).

45. C. R. Carlson, B. Lygren, T. Berge, N. Hoshi, W. Wong, K. Taskén, J. D. Scott, Delineation of type I protein kinase A-selective signaling events using an RI anchoring disruptor. *J. Biol. Chem.* **281**, 21535–21545 (2006).
46. A. J. Stokka, R. Mosenden, A. Ruppelt, B. Lygren, K. Taskén, The adaptor protein EBP50 is important for localization of the protein kinase A-Ezrin complex in T-cells and the immunomodulating effect of cAMP. *Biochem. J.* **425**, 381–388 (2010).
47. K. W. Brudvik, K. Henjum, E. M. Aandahl, B. A. Bjørnbeth, K. Taskén, Regulatory T-cell-mediated inhibition of antitumor immune responses is associated with clinical outcome in patients with liver metastasis from colorectal cancer. *Cancer Immunol. Immunother.* **61**, 1045–1053 (2012).
48. D. Wang, R. N. DuBois, Immunosuppression associated with chronic inflammation in the tumor microenvironment. *Carcinogenesis* **36**, 1085–1093 (2015).
49. X. Qian, L. Gu, H. Ning, Y. Zhang, E. C. Hsueh, M. Fu, X. Hu, L. Wei, D. F. Hoft, J. Liu, Increased Th17 cells in the tumor microenvironment is mediated by IL-23 via tumor-secreted prostaglandin E2. *J. Immunol.* **190**, 5894–5902 (2013).
50. C. Yao, D. Sakata, Y. Esaki, Y. Li, T. Matsuoka, K. Kuroiwa, Y. Sugimoto, S. Narumiya, Prostaglandin E2-EP4 signaling promotes immune inflammation through Th1 cell differentiation and Th17 cell expansion. *Nat. Med.* **15**, 633–640 (2009).
51. J. Lee, T. Aoki, D. Thumkeo, R. Siriwach, C. Yao, S. Narumiya, T cell–intrinsic prostaglandin E_2-EP2/EP4 signaling is critical in pathogenic T_H17 cell–driven inflammation. *J. Allergy Clin. Immunol.* **143**, 631–643 (2018).
52. P. Krause, M. Bruckner, C. Uermösi, E. Singer, M. Groettrup, D. F. Legler, Prostaglandin E_2 enhances T-cell proliferation by inducing the costimulatory molecules OX40L, CD70, and 4-1BBL on dendritic cells. *Blood* **113**, 2451–2460 (2009).
53. N. G. Oberprieler, S. Lemeer, M. E. Kalland, K. M. Torgersen, A. J. R. Heck, K. Taskén, High-resolution mapping of prostaglandin E2-dependent signaling networks identifies a constitutively active PKA signaling node in CD8+CD45RO+ T cells. *Blood* **116**, 2253–2265 (2010).
54. P. Giansanti, M. P. Stokes, J. C. Silva, A. Scholten, A. J. R. Heck, Interrogating cAMP-dependent kinase signaling in Jurkat T cells via a protein kinase A targeted immune-precipitation phosphoproteomics approach. *Mol. Cell. Proteomics* **12**, 3350–3359 (2013).
55. E. L. de Graaf, P. Giansanti, A. F. M. Altelaar, A. J. R. Heck, Single-step enrichment by Ti4+-IMAC and label-free quantitation enables in-depth monitoring of phosphorylation dynamics with high reproducibility and temporal resolution. *Mol. Cell. Proteomics* **13**, 2426–2434 (2014).
56. C. Gerarduzzi, Q. W. He, J. Antoniou, J. A. di Battista, Quantitative phosphoproteomic analysis of signaling downstream of the prostaglandin e2/g-protein coupled receptor in human synovial fibroblasts: Potential antifibrotic networks. *J. Proteome Res.* **13**, 5262–5280 (2014).
57. M. A. Gavin, J. P. Rasmussen, J. D. Fontenot, V. Vasta, V. C. Manganiello, J. A. Beavo, A. Y. Rudensky, Foxp3-dependent programme of regulatory T-cell differentiation. *Nature* **445**, 771–775 (2007).
58. H. Horn, E. M. Schoof, J. Kim, X. Robin, M. L. Miller, F. Diella, A. Palma, G. Cesareni, L. J. Jensen, R. Linding, KinomeXplorer: An integrated platform for kinome biology studies. *Nat. Methods* **11**, 603–604 (2014).
59. J. A. Ubersax, J. E. Ferrell Jr., Mechanisms of specificity in protein phosphorylation. *Nat. Rev. Mol. Cell Biol.* **8**, 530–541 (2007).
60. T. Purzner, J. Purzner, T. Buckstaff, G. Cozza, S. Gholamin, J. M. Rusert, T. A. Hartl, J. Sanders, N. Conley, X. Ge, M. Langan, V. Ramaswamy, L. Ellis, U. Litzenburger, S. Bolin, J. Theruvath, R. Nitta, L. Qi, X. N. Li, G. Li, M. D. Taylor, R. J. Wechsler-Reya, L. A. Pinna, Y. J. Cho, M. T. Fuller, J. E. Elias, M. P. Scott, Developmental phosphoproteomics identifies the kinase CK2 as a driver of Hedgehog signaling and a therapeutic target in medulloblastoma. *Sci. Signal.* **11**, eaau5147 (2018).
61. Q. Xiao, B. Miao, J. Bi, Z. Wang, Y. Li, Prioritizing functional phosphorylation sites based on multiple feature integration. *Sci. Rep.* **6**, 24735 (2016).
62. J. Landskron, K. Tasken, Phosphoprotein detection by high-throughput flow cytometry. *Methods Mol. Biol.* **1355**, 275–290 (2016).
63. X. Fang, S. X. Yu, Y. Lu, R. C. Bast, J. R. Woodgett, G. B. Mills, Phosphorylation and inactivation of glycogen synthase kinase 3 by protein kinase A. *Proc. Natl. Acad. Sci. U.S.A.* **97**, 11960–11965 (2000).
64. J. K. Wentworth, G. Pula, A. W. Poole, Vasodilator-stimulated phosphoprotein (VASP) is phosphorylated on Ser157 by protein kinase C-dependent and -independent mechanisms in thrombin-stimulated human platelets. *Biochem. J.* **393**, 555–564 (2006).
65. J. E. Eriksson, T. He, A. V. Trejo-Skalli, A.-S. Härmälä-Braskén, J. Hellman, Y.-H. Chou, R. D. Goldman, Specific in vivo phosphorylation sites determine the assembly dynamics of vimentin intermediate filaments. *J. Cell Sci.* **117**, 919–932 (2004).
66. A. Sawicka, C. Seiser, Histone H3 phosphorylation - A versatile chromatin modification for different occasions. *Biochimie* **94**, 2193–2201 (2012).
67. A. Y. Wen, K. M. Sakamoto, L. S. Miller, The role of the transcription factor CREB in immune function. *J. Immunol.* **185**, 6413–6419 (2010).
68. S. Kostenko, U. Moens, Heat shock protein 27 phosphorylation: Kinases, phosphatases, functions and pathology. *Cell. Mol. Life Sci.* **66**, 3289–3307 (2009).
69. M. R. Elliott, R. A. Shanks, I. U. Khan, J. W. Brooks, P. J. Burkett, B. J. Nelson, V. Kyttaris, Y. T. Juang, G. C. Tsokos, G. M. Kammer, Down-regulation of IL-2 production in T lymphocytes by phosphorylated protein kinase A-RIIβ. *J. Immunol.* **172**, 7804–7812 (2004).
70. S. Manni, J. H. Mauban, C. W. Ward, M. Bond, Phosphorylation of the cAMP-dependent protein kinase (PKA) regulatory subunit modulates PKA-AKAP interaction, substrate phosphorylation, and calcium signaling in cardiac cells. *J. Biol. Chem.* **283**, 24145–24154 (2008).
71. R. D. Cauthron, K. B. Carter, S. Liauw, R. A. Steinberg, Physiological phosphorylation of protein kinase A at Thr-197 is by a protein kinase A kinase. *Mol. Cell. Biol.* **18**, 1416–1423 (1998).
72. M. J. Moore, J. R. Kanter, K. C. Jones, S. S. Taylor, Phosphorylation of the catalytic subunit of protein kinase A. Autophosphorylation versus phosphorylation by phosphoinositide-dependent kinase-1. *J. Biol. Chem.* **277**, 47878–47884 (2002).
73. K. Senarath, D. Kankanamge, S. Samaradivakara, K. Ratnayake, M. Tennakoon, A. Karunarathne, Regulation of G protein βγ signaling. *Int. Rev. Cell Mol. Biol.* **339**, 133–191 (2018).
74. S. M. Khan, R. Sleno, S. Gora, P. Zylbergold, J. P. Laverdure, J. C. Labbé, G. J. Miller, T. E. Hébert, The expanding roles of Gβγ subunits in G protein-coupled receptor signaling and drug action. *Pharmacol. Rev.* **65**, 545–577 (2013).
75. A. V. Smrcka, G protein βγ subunits: Central mediators of G protein-coupled receptor signaling. *Cell. Mol. Life Sci.* **65**, 2191–2214 (2008).
76. Y. K. Peterson, L. M. Luttrell, The diverse roles of arrestin scaffolds in G protein-coupled receptor signaling. *Pharmacol. Rev.* **69**, 256–297 (2017).
77. P. Y. Jean-Charles, S. Kaur, S. K. Shenoy, G protein-coupled receptor signaling through β-arrestin-dependent mechanisms. *J. Cardiovasc. Pharmacol.* **70**, 142–158 (2017).
78. J. T. Murray, D. G. Campbell, N. Morrice, G. C. Auld, N. Shpiro, R. Marquez, M. Peggie, J. Bain, G. B. Bloomberg, F. Grahammer, F. Lang, P. Wulff, D. Kuhl, P. Cohen, Exploitation of KESTREL to identify NDRG family members as physiological substrates for SGK1 and GSK3. *Biochem. J.* **384**, 477–488 (2004).
79. Y. M. Oh, H. B. Park, J. H. Shin, J. E. Lee, H. Y. Park, D. H. Kho, J. S. Lee, H. Choi, T. Okuda, K. Kokame, T. Miyata, I. H. Kim, S. H. Lee, R. H. Schwartz, K. Choi, Ndrg1 is a T-cell clonal anergy factor negatively regulated by CD28 costimulation and interleukin-2. *Nat. Commun.* **6**, 8698 (2015).
80. P. P. Roux, D. Shahbazian, H. Vu, M. K. Holz, M. S. Cohen, J. Taunton, N. Sonenberg, J. Blenis, RAS/ERK signaling promotes site-specific ribosomal protein S6 phosphorylation via RSK and stimulates cap-dependent translation. *J. Biol. Chem.* **282**, 14056–14064 (2007).
81. M. C. Veri, K. E. DeBell, M. C. Seminario, A. DiBaldassarre, I. Reischl, R. Rawat, L. Graham, C. Noviello, B. L. Rellahan, S. Miscia, R. L. Wange, E. Bonvini, Membrane raft-dependent regulation of phospholipase Cgamma-1 activation in T lymphocytes. *Mol. Cell. Biol.* **21**, 6939–6950 (2001).
82. D. Beach, R. Gonen, Y. Bogin, I. G. Reischl, D. Yablonski, Dual role of SLP-76 in mediating T cell receptor-induced activation of phospholipase C-γ1. *J. Biol. Chem.* **282**, 2937–2946 (2007).
83. Z. Dong, A. M. Bode, The role of histone H3 phosphorylation (Ser10 and Ser28) in cell growth and cell transformation. *Mol. Carcinog.* **45**, 416–421 (2006).
84. P. Siripurapu, D. Kankanamge, K. Ratnayake, K. Senarath, A. Karunarathne, Two independent but synchronized Gβγ subunit-controlled pathways are essential for trailing-edge retraction during macrophage migration. *J. Biol. Chem.* **292**, 17482–17495 (2017).
85. C. R. Surve, D. Lehmann, A. V. Smrcka, A chemical biology approach demonstrates G protein βγ subunits are sufficient to mediate directional neutrophil chemotaxis. *J. Biol. Chem.* **289**, 17791–17801 (2014).
86. G. L. Christensen, C. D. Kelstrup, C. Lyngsø, U. Sarwar, R. Bøgebo, S. P. Sheikh, S. Gammeltoft, J. V. Olsen, J. L. Hansen, Quantitative phosphoproteomics dissection of seven-transmembrane receptor signaling using full and biased agonists. *Mol. Cell. Proteomics* **9**, 1540–1553 (2010).
87. K. Du, M. Montminy, CREB is a regulatory target for the protein kinase Akt/PKB. *J. Biol. Chem.* **273**, 32377–32379 (1998).
88. C. D. Terfve, E. H. Wilkes, P. Casado, P. R. Cutillas, J. Saez-Rodriguez, Large-scale models of signal propagation in human cells derived from discovery phosphoproteomic data. *Nat. Commun.* **6**, 8033 (2015).
89. N. M. Riley, J. J. Coon, Phosphoproteomics in the age of rapid and deep proteome profiling. *Anal. Chem.* **88**, 74–94 (2016).
90. C. Álvarez-Salamero, R. Castillo-González, M. N. Navarro, Lighting up T lymphocyte signaling with quantitative phosphoproteomics. *Front. Immunol.* **8**, 938 (2017).
91. M. G. Beltejar, H.-T. Lau, M. G. Golkowski, S.-E. Ong, J. A. Beavo, Analyses of PDE-regulated phosphoproteomes reveal unique and specific cAMP-signaling modules in T cells. *Proc. Natl. Acad. Sci. U.S.A.* **114**, E6240–E6249 (2017).

92. E. J. Needham, B. L. Parker, T. Burykin, D. E. James, S. J. Humphrey, Illuminating the dark phosphoproteome. *Sci. Signal.* **12**, eaau8645 (2019).
93. J. Bain, L. Plater, M. Elliott, N. Shpiro, C. J. Hastie, H. Mclauchlan, I. Klevernic, J. S. C. Arthur, D. R. Alessi, P. Cohen, The selectivity of protein kinase inhibitors: A further update. *Biochem. J.* **408**, 297–315 (2007).
94. A. Lochner, J. A. Moolman, The many faces of H89: A review. *Cardiovasc. Drug Rev.* **24**, 261–274 (2006).
95. S. A. Gibson, E. N. Benveniste, Protein kinase CK2: An emerging regulator of immunity. *Trends Immunol.* **39**, 82–85 (2018).
96. T. Kobayashi, Y. Nakatani, T. Tanioka, M. Tsujimoto, S. Nakajo, K. Nakaya, M. Murakami, I. Kudo, Regulation of cytosolic prostaglandin E synthase by phosphorylation. *Biochem. J.* **381**, 59–69 (2004).
97. R. Yefi, D. P. Ponce, I. Niechi, E. Silva, P. Cabello, D. A. Rodriguez, K. Marcelain, R. Armisen, A. F. G. Quest, J. C. Tapia, Protein kinase CK2 promotes cancer cell viability via up-regulation of cyclooxygenase-2 expression and enhanced prostaglandin E2 production. *J. Cell. Biochem.* **112**, 3167–3175 (2011).
98. S. F. Greer, Y. N. Wang, C. Raman, L. B. Justement, CD45 function is regulated by an acidic 19-amino acid insert in domain II that serves as a binding and phosphoacceptor site for casein kinase 2. *J. Immunol.* **166**, 7208–7218 (2001).
99. H. Abrahamsen, T. Vang, K. Tasken, Protein kinase A intersects SRC signaling in membrane microdomains. *J. Biol. Chem.* **278**, 17170–17177 (2003).
100. M. Krause, E. W. Dent, J. E. Bear, J. J. Loureiro, F. B. Gertler, Ena/VASP proteins: Regulators of the actin cytoskeleton and cell migration. *Annu. Rev. Cell Dev. Biol.* **19**, 541–564 (2003).
101. J. M. Chemnitz, J. Driesen, S. Classen, J. L. Riley, S. Debey, M. Beyer, A. Popov, T. Zander, J. L. Schultze, Prostaglandin E2 impairs CD4+ T cell activation by inhibition of lck: Implications in Hodgkin's lymphoma. *Cancer Res.* **66**, 1114–1122 (2006).
102. K. Kabashima, T. Saji, T. Murata, M. Nagamachi, T. Matsuoka, E. Segi, K. Tsuboi, Y. Sugimoto, T. Kobayashi, Y. Miyachi, A. Ichikawa, S. Narumiya, The prostaglandin receptor EP4 suppresses colitis, mucosal damage and CD4 cell activation in the gut. *J. Clin. Investig.* **109**, 883–893 (2002).
103. S. Desai, H. April, C. Nwaneshiudu, B. Ashby, Comparison of agonist-induced internalization of the human EP2 and EP4 prostaglandin receptors: Role of the carboxyl terminus in EP4 receptor sequestration. *Mol. Pharmacol.* **58**, 1279–1286 (2000).
104. H. Fujino, S. Salvi, J. W. Regan, Differential regulation of phosphorylation of the cAMP response element-binding protein after activation of EP2 and EP4 prostanoid receptors by prostaglandin E2. *Mol. Pharmacol.* **68**, 251–259 (2005).
105. M. D. Castellone, H. Teramoto, B. O. Williams, K. M. Druey, J. S. Gutkind, Prostaglandin E2 promotes colon cancer cell growth through a Gs-Axin-β-Catenin signaling axis. *Science* **310**, 1504–1510 (2005).
106. K. W. Brudvik, J. E. Paulsen, E. M. Aandahl, B. Roald, K. Taskén, Protein kinase A antagonist inhibits β-catenin nuclear translocation, c-Myc and COX-2 expression and tumor promotion in ApcMin/+ mice. *Mol. Cancer* **10**, 149 (2011).
107. S. Y. Cheng, H. Zhang, M. Zhang, S.-K. Xia, X.-M. Bai, L. Zhang, J. Ma, R. Rong, Y.-P. Wang, M.-Z. Du, J. Wang, M. Chen, F. Shi, Q.-Y. Yang, J. Leng, Prostaglandin E_2 receptor EP2 mediates Snail expression in hepatocellular carcinoma cells. *Oncol. Rep.* **31**, 2099–2106 (2014).
108. F. Neuschäfer-Rube, R. Hermosilla, M. Kuna, A. Pathe-Neuschäfer-Rube, R. Schülein, G. P. Püschel, A Ser/Thr cluster within the C-terminal domain of the rat prostaglandin receptor EP3αis essential for agonist-induced phosphorylation, desensitization and internalization. *Br. J. Pharmacol.* **145**, 1132–1142 (2005).
109. E. V. Gurevich, J. J. G. Tesmer, A. Mushegian, V. V. Gurevich, G protein-coupled receptor kinases: more than just kinases and not only for GPCRs. *Pharmacol. Ther.* **133**, 40–69 (2012).
110. H. Zhang, S. Cheng, M. Zhang, X. Ma, L. Zhang, Y. Wang, R. Rong, J. Ma, S. Xia, M. Du, F. Shi, J. Wang, Q. Yang, X. Bai, J. Leng, Prostaglandin E2 promotes hepatocellular carcinoma cell invasion through upregulation of YB-1 protein expression. *Int. J. Oncol.* **44**, 769–780 (2014).
111. M. Z. Du, F. Shi, H. Zhang, S. Xia, M. Zhang, J. Ma, X. Bai, L. Zhang, Y. Wang, S. Cheng, Q. Yang, J. Leng, Prostaglandin E2 promotes human cholangiocarcinoma cell proliferation, migration and invasion through the upregulation of β-catenin expression via EP3-4 receptor. *Oncol. Rep.* **34**, 715–726 (2015).
112. Z. X. Wang, Transactivation of epidermal growth factor receptor by G protein-coupled receptors: Recent progress, challenges and future research. *Int. J. Mol. Sci.* **17**, 95 (2016).
113. H. Zhou, M. Ye, J. Dong, E. Corradini, A. Cristobal, A. J. R. Heck, H. Zou, S. Mohammed, Robust phosphoproteome enrichment using monodisperse microsphere-based immobilized titanium (IV) ion affinity chromatography. *Nat. Protoc.* **8**, 461–480 (2013).
114. J. Rappsilber, Y. Ishihama, M. Mann, Stop and go extraction tips for matrix-assisted laser desorption/ionization, nanoelectrospray, and LC/MS sample pretreatment in proteomics. *Anal. Chem.* **75**, 663–670 (2003).
115. C. K. Frese, A. F. M. Altelaar, M. L. Hennrich, D. Nolting, M. Zeller, J. Griep-Raming, A. J. R. Heck, S. Mohammed, Improved peptide identification by targeted fragmentation using CID, HCD and ETD on an LTQ-Orbitrap Velos. *J. Proteome Res.* **10**, 2377–2388 (2011).
116. J. Cox, M. Mann, MaxQuant enables high peptide identification rates, individualized p.p.b.-range mass accuracies and proteome-wide protein quantification. *Nat. Biotechnol.* **26**, 1367–1372 (2008).
117. S. Tyanova, T. Temu, P. Sinitcyn, A. Carlson, M. Y. Hein, T. Geiger, M. Mann, J. Cox, The Perseus computational platform for comprehensive analysis of (prote)omics data. *Nat. Methods* **13**, 731–740 (2016).
118. R Development Core Team, R: A Language and Environment for Statistical Computing (Vienna Austria R Found. Stat. Comput, 2008), vol. 1.
119. N. Colaert, K. Helsens, L. Martens, J. Vandekerckhove, K. Gevaert, Improved visualization of protein consensus sequences by iceLogo. *Nat. Methods* **6**, 786–787 (2009).
120. G. Bindea, B. Mlecnik, H. Hackl, P. Charoentong, M. Tosolini, A. Kirilovsky, W. H. Fridman, F. Pagès, Z. Trajanoski, J. Galon, ClueGO: A cytoscape plug-in to decipher functionally grouped gene ontology and pathway annotation networks. *Bioinformatics* **25**, 1091–1093 (2009).
121. J. A. Vizcaíno, R. G. Côté, A. Csordas, J. A. Dianes, A. Fabregat, J. M. Foster, J. Griss, E. Alpi, M. Birim, J. Contell, G. O'Kelly, A. Schoenegger, D. Ovelleiro, Y. Pérez-Riverol, F. Reisinger, D. Ríos, R. Wang, H. Hermjakob, The PRoteomics IDEntifications (PRIDE) database and associated tools: Status in 2013. *Nucleic Acids Res.* **41** (Database issue), D1063–D1069 (2013).
122. D. Türei, T. Korcsmáros, J. Saez-Rodriguez, OmniPath: Guidelines and gateway for literature-curated signaling pathway resources. *Nat. Methods* **13**, 965–967 (2016).
123. A. Liberzon, C. Birger, H. Thorvaldsdóttir, M. Ghandi, J. P. Mesirov, P. Tamayo, The molecular signatures database hallmark gene set collection. *Cell Syst.* **1**, 417–425 (2015).
124. M. Miyara, Y. Yoshioka, A. Kitoh, T. Shima, K. Wing, A. Niwa, C. Parizot, C. Taflin, T. Heike, D. Valeyre, A. Mathian, T. Nakahata, T. Yamaguchi, T. Nomura, M. Ono, Z. Amoura, G. Gorochov, S. Sakaguchi, Functional delineation and differentiation dynamics of human CD4+ T cells expressing the FoxP3 transcription factor. *Immunity* **30**, 899–911 (2009).

Acknowledgments: We thank J. Solheim and J. Landskron for practical assistance with and advice on the methylation studies. We further thank T. Maruyama at ONO Pharmaceutical Co. Ltd. for providing EP receptor agonists and antagonists. **Funding:** The work was supported by grants from the Norwegian Cancer Society (grant no. 182794 and 215850), The Regional Health Authority for South-Eastern Norway (grant no. 2017119), the Research Council of Norway (grant no. 187615 and 294916), Stiftelsen Kristian Gerhard Jebsen (grant no. SKGJ-MED-09 and SKGJ-MED-19), and the European Union Horizon 2020 program INFRAIA project Epic-XS (project 823839). E. Gjerga and A. Dugourd were supported by the European Union's Horizon 2020 research and innovation programme (675585 Marie-Curie ITN "SymBioSys") and the JRC for Computational Biomedicine, which was partially funded by Bayer. **Author contributions:** K.T. and A.M.L. conceived the study. A.M.L., M.J.J., and P.G. performed experiments. A.M.L., M.J.J., and P.G. analyzed the data. E.G. and A.D. performed mathematical modeling. K.T., A.S., J.S.-R., and A.J.R.H. supervised the work. A.M.L., P.G., and E.G. wrote the paper. All authors commented on the manuscript and approved the final version. **Competing interests:** J.S.-R. receives funding from Glaxo-Smith-Kline and Sanofi and consultant fees from Travere Therapeutics. The authors declare that they have no other competing interests. **Data and materials availability:** The MS proteomics data have been deposited in the ProteomeXchange Consortium through the PRIDE partner repository with the dataset identifier PXD014503. The EP_{1-4} agonists and antagonists were provided by ONO Pharmaceuticals under a material transfer agreement. All other data needed to evaluate the conclusions in the paper are present in the paper and/or the Supplementary Materials.

Submitted 20 May 2020
Accepted 9 September 2021
Published 5 October 2021
10.1126/scisignal.abc8579

Citation: A. M. Lone, P. Giansanti, M. J. Jørgensen, E. Gjerga, A. Dugourd, A. Scholten, J. Saez-Rodriguez, A. J. R. Heck, K. Taskén, Systems approach reveals distinct and shared signaling networks of the four PGE_2 receptors in T cells. *Sci. Signal.* **14**, eabc8579 (2021).

Science Signaling

Systems approach reveals distinct and shared signaling networks of the four PGE receptors in T cells

Anna M. LonePiero GiansantiMarthe Jøntvedt JørgensenEnio GjergaAurelien DugourdArjen ScholtenJulio Saez-RodriguezAlbert J. R. HeckKjetil Taskén

Sci. Signal., 14 (703), eabc8579. • DOI: 10.1126/scisignal.abc8579

PGE2 signaling networks

The lipid mediator PGE suppresses antitumor immunity by activating its four related GPCRs on T cells. Lone *et al.* used quantitative phosphoproteomics and phosphoflow cytometry to analyze downstream signaling elicited by the stimulation of all receptors simultaneously or individually in different T cell subsets. The analysis revealed G protein–dependent and G protein–independent pathways that were activated by each receptor in all T cells, as well as pathways that were activated by only a subset of receptors, in only a subset of cells, or with receptor-specific kinetics. Network modeling predicted mechanisms of cross-talk and signal integration downstream of the receptors. These data are a comprehensive resource for future explorations of the functional consequences of PGE receptor–specific signaling in immune homeostasis, inflammation, and tumor-associated immunosuppression.

Science Signaling (ISSN) is published by the American Association for the Advancement of Science. 1200 New York Avenue NW, Washington, DC 20005. The title *Science Signaling* is a registered trademark of AAAS.